North Dakota State University

Graduate School

Title

NEURAL SYNCHRONY AND ASYNCHRONY AS MECHANISMS FOR PERCEPTUAL GROUPING AND SEGMENTATION

By

Aaron Clarke

The Supervisory Committee certifies that this *disquisition* complies with North Dakota State University's regulations and meets the accepted standards for the degree of

DOCTOR OF PHILOSOPHY

ABSTRACT

Clarke, Aaron, Ph.D., Department of Psychology, College of Science and Mathematics, North Dakota State University, July 2010. Neural Synchrony and Asynchrony as Mechanisms for Perceptual Grouping and Segmentation. Major Professor: Dr. Stéphane Rainville.

The question of whether neural synchrony has functional significance for cortical processing has been an issue of contention in the recent scientific literature. Although the balance of evidence now seems to be favoring a view that synchrony does indeed play a significant functional role, this role's mechanisms and its behavioral consequences have not been fully elucidated. In this research I add to the growing body of evidence in favor of a significant functional role for neural synchrony in cortical processing. By leveraging a modified version of Cheadle, Bauer, Parton, Müller, Bonneh and Usher (2008)'s psychophysical paradigm and through experiments of my own design, I find evidence suggesting that when contrast oscillations serve as inputs to the visual system, the system produces behavior that may be more synchronous than the stimulus or less synchronous than the stimulus depending on whether or not the oscillations occur on elements of a common object or on elements of separate objects respectively. The current paradigm has the potential to test behavioral manifestations of the underlying neural dynamics that heretofore were largely thought to be confined to physiological measures. Furthermore, I provide a biophysical model that predicts this behavior and other related electrophysiological findings.

ACKNOWLEDGMENTS

This dissertation would never have been possible without the loyal support of my family and friends. In particular, my mother and father have been untiring aids to me throughout my academic career. My sisters Amy and Sarah have always been there for me whenever I needed them. My grandma and grandpa Clarke have shown no end to their support for me.

I would also like to thank Yamaya Sosa, Hsin-Mei Sun, Lindsey Leeker, Nora Gayzur, Jonathon George, Alyson Saville, Daniel Reetz, Lyle Stramer, Wolfgang Teder, Yaniv Morgenstern, Charles Or, Bob Hou, Ian Chung, Fridolin Ting and Sonya Dykstra for being some of the best friends a guy could ask for.

My advisor, Stéphane Rainville was a friend long before he became my advisor, and I look forward to our continued friendship in the years to come. He has been a great sounding board for my ideas, he has steered me in new and interesting directions, and his kindness and generosity are overwhelming.

Finally, I am deeply indebted to my committee for their kindness and understanding in helping my get through all of the red tape and growing pains that go along with doing a dissertation. Thanks to Mark McCourt for letting me bounce ideas off of him in Stéphane's absence and for all of the cool side-projects he has let me get involved in. Thanks to Mark Nawrot for his diligent revisions on my manuscripts and for inviting me to share American Thanksgiving with him and his family every year. Thanks to Clayton Hilmert for providing a unique perspective on my dissertation and for several fun games of Texas Hold'em and sushi lunches, and thanks to Brian Slator for Artificial Intelligence and for inspiring conversations at the Turf.

TABLE OF CONTENTS

LIST OF TABLES

LIST OF FIGURES

CHAPTER 1. INTRODUCTION

In this dissertation I will discuss many topics where the reader's comprehension will depend on a fundamental understanding of basic vision. As such, I have designed this document to progress from a basic review of vision science to a more sophisticated exposition of the topic of interest (mainly neural synchrony). During this process I will discuss spatial vision, temporal vision, joint spatiotemporal vision (including vision for motion). pattern vision and neural synchrony. After providing the necessary level of background knowledge I will weave together the thesis of this document, that cortical synchrony may be involved in encoding spatial relationships and that a plausible mechanism using synchrony may be modeled using networked Hodgkin and Huxley neurons.

1.1. Spatial Vision

The term *spatial vision* generally refers to vision for static scenes. Although it is now known that the visual system integrates spatial and temporal information simultaneously (Adelson and Bergen, 1985; Heeger, 1987; Simoncelli and Heeger, 1998), historically, there have been many papers published where these two topics are treated separately. This first section will thus focus spatial vision in its own right. There are literally thousands of articles published on spatial vision. The following review shall focus in detail on some of the foundational and most influential papers in this area that are of relevance to the current research.

1.1.1. The Eyes

Spatial vision begins with the eyes. Light from the world enters the eyes through the pupils and is focused at the backs of the eyes through their lenses. The back of each eye is covered with a layer of light-sensitive cells called photoreceptors that are sensitive to the impinging light's wavelength, intensity and spatial distribution.

There are at least two kinds of photoreceptors: rods and cones, with cones being divisible into three sub-categories depending on whether they are maximally sensitive to long, medium or short wavelength light (corresponding roughly to percepts of red, green and blue) (Burns and Lamb, 2004). Cones are primarily concentrated in a densely packed region of the retina called the fovea, providing high resolution daytime vision (or *photopic* vision), while rods predominate in the areas peripheral to the fovea, providing lower resolution night time vision (or *scotopic* vision). Cones are fast acting and have a temporal integration window of about 50 msec, while rods are slower acting and have a temporal integration window of about 300 msec (Sterling, 2004). Signals from the photoreceptors pass through a complex network of neurons within the retina that spatially pool information over small regions of the visual field (Sterling, 2004). Part of this network's function seems to be involved in regulating sensitivity to light signals as a function of the average luminance in the environment (Sterling, 2004). Furthermore, the retinal neural network splits information into at least three streams based on three main classes of retinal ganglion cells: parasol, midget and bistratified ganglion cells. The parasol ganglion cells pass information integrated over many photoreceptors to higher levels of the visual system following a fast, myelinated pathway called the magnocellular pathway (Kandel et al., 2000). The midget ganglion cells, conversely, integrate information over a relatively fewer photoreceptors and send their signals through a slower pathway called the parvocellular pathway (Kandel et al., 2000). The bistratified ganglion cells integrate information over an intermediate number of rods and cones and send their signals through a moderate conduction velocity pathway called the koniocellular pathway (Rodieck, 1991; Dacey, 1993). The three pathways magnocellular, parvocellular and koniocellular (or m, p and k for short) are fairly well differentiated and anatomically distinct in the next neural relay station following the retina - the lateral geniculate

nucleus (or LGN).

1.1.2. Lateral Geniculate Nucleus

Within the LGN neural responses are retinotopically mapped, meaning that if two neurons are adjacent in the retina then the corresponding LGN neurons that they activate are also adjacent. LGN neurons respond selectively when the organism sees light in a particular part of its visual field and not when the light is in any other part of the visual field. The area of the visual field over which the neuron will respond is called its *receptive field.* Some LGN neurons have receptive fields that prefer stimuli with light in the middle and darkness in the surround. These are called on-center-off-surround receptive fields. Other LGN neurons have receptive fields that prefer stimuli with darkness in the middle and light in the surrounds. These are called off-center-on-surround receptive fields. Both receptive field types are circularly symmetric. Importantly, both retinal and LGN neural responses are time-locked to the incoming light patterns (Sherman, 1996, 2001). This means that spatial and temporal relationships existing in the external light field are preserved in the early internal representations of the light field. By filtering the retinal image with LGN receptive fields, the visual system essentially highlights contrast in an image, independently image's average luminance.

1.1.3. Primary Visual Cortex

Like LGN neurons, primary visual cortex neurons are also retinotopically mapped and have receptive fields. Unlike LGN neurons, however, primary visual cortex (V1) neurons have receptive fields that are selective for orientation, spatial frequency, temporal frequency, color and binocular disparity (Hubel and Wiesel, 1962, 1968; De Valois et al., 1982) (see Figure 1). The V1 receptive fields reported by Hubel and Wiesel (1962) are presented in Figure 2. Hubel and Wiesel (1962) proposed that V1 receptive fields selectively pool inputs from LGN receptive fields as shown in Figure

3. This model is still widely accepted today (Stork and Wilson, 1990).

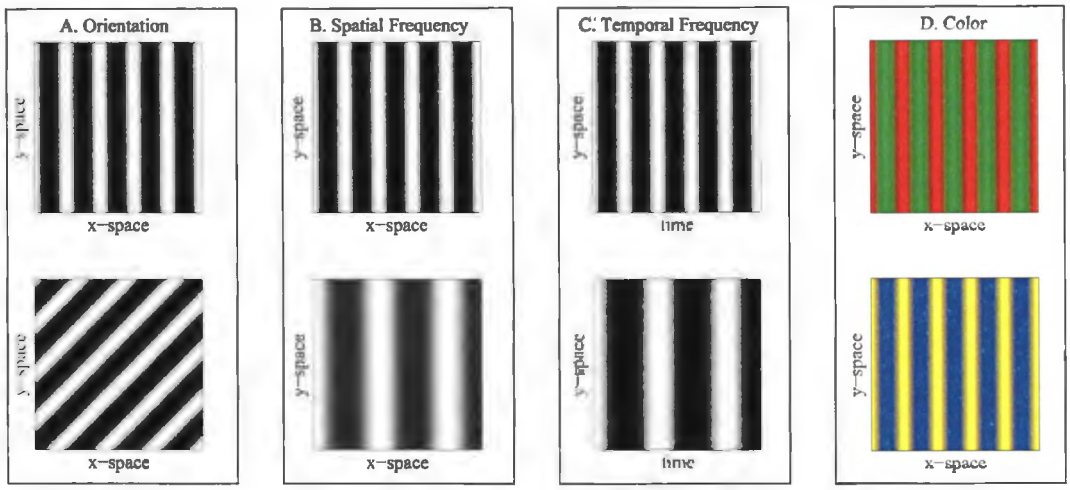

Figure 1. Examples of gratings having A: different orientations, B: different spatial frequencies, C: different temporal frequencies and D: different colors.

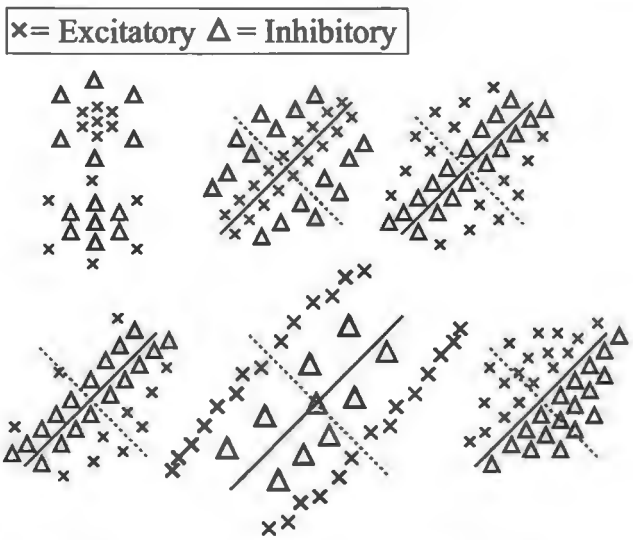

Figure 2. Example receptive fields reported by Hubel and Weisel (1962). Excitatory regions respond preferentially to increased illumination whereas inhibitory regions respond preferentially to decreased illumination.

In the process of describing V1 neurons' behavior Hubel and Wiesel (1962, 1968) noticed that V1 RF's tended to fall into two general classes that they called simple and complex. Simple cells were classified based on having RF's that (a) possessed well demarcated regions preferentially responding to light or dark stimulation (b) summing responses within those regions and (c) allowing one to qualitatively predict responses

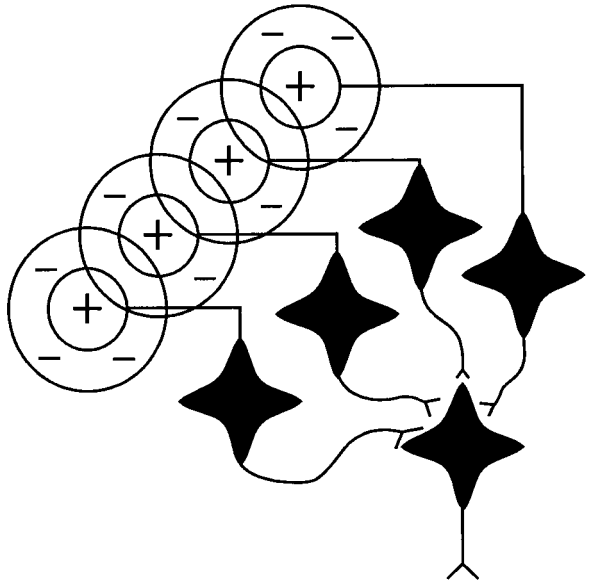

Figure 3. Illustration of receptive field formation in V1 based on LGN inputs. Circularly symmetric LGN neurons that are spatially distributed so as to fall along a straight line make converging connections with a single V1 cell - thereby conferring that cell with orientation selectivity.

to moving or flashing stimuli within those regions. Complex cell responses were classified as (a) failing to demonstrate the aforementioned properties and (b) generally showing a mixture of light and dark stimulation preference across their RFs. They also found "Hypercomplex" cells, which were classified based on demonstrating end-zone inhibition. Lastly, they found some cells with little or no orientation selectivity (Hubel and Wiesel, 1962).

Simple and complex cell responses were more extensively investigated by De Valois et al. (1982). De Valois et al. (1982) found that simple cells responded to a sine wave grating drifting across their RF by changing their firing rate in a way that was spatially and temporally phase locked with, and at the same frequency as the drifting grating. A cell can not fire less than zero spikes/second, so during the negative phase of the grating's drift the cell's responses simply remained at zero (i.e. they showed half-wave rectification). In a small number of cases the simple cells were found to have a non-zero mean firing rate. These cells demonstrated a decrease in

responsiveness below the mean firing rate in response to the negative phase of the drifting grating. De Valois et al. (1982) also found that simple cells have an almost zero spikes/second response to a uniform gray field (0.25 spikes/sec).

Complex cells, on the other hand were found to have a sustained response to a drifting sine wave grating while maintaining a near zero spikes/second response to a uniform gray field. De Valois et al. (1982) noted that, for complex cells, the predominant harmonic response to stimulation by a given frequency was twice the flicker frequency. This phenomenon is called frequency doubling and implies that complex cells respond equally to the white and black bars of the grating independently of their position (i.e. their responses are invariant with respect to contrast polarity).

De Valois et al. (1982) found that simple and complex cell bandwidths vary roughly uniformly over a range from 0.6 to 2.5 octaves and that this range is consistent from the fovea to the parafovea. They found spatial frequency selectivity to range continuously from less than half of a degree of visual angle to more than sixteen degrees of visual angle. Wilson (1978) had suggested that behaviorally obtained spatial frequency contrast sensitivity functions may be adequately modeled using just three or four different tuning functions. De Valois et al. (1982)'s results, however, suggested that this was not true of the underlying neural populations mediating the contrast response function, where many individual neurons had spatial frequency selectivity that spanned a relatively narrow range and covered overlapping regions of the spatial frequency spectrum.

De Valois et al. (1982)'s research implies that a minimal description of V1 neural receptive fields characterizes them in at least in terms of a wavelet transform. Gabor (1946) provided the quintessential formulation of a wavelet transform and Figure 4 shows examples of the kinds of wavelets he originated. Since Gabor's time, however, several more flavors of wavelets have come on the scene (such as the difference of

Figure 4. Example Gabors. These two Gabors differ in their orientation, spatial frequency and phase.

Gaussians. the derivative of Gaussian, the oriented different of Gaussians and the balanced Gabor) and evidence suggests that Gabor's wavelets need to be modified in order to accurately model V1 neural responses, with perhaps the best fitting function being the balanced Gabor (Stork and Wilson, 1990; Blakeslee and McCourt, 1999; Cope et al., 2008).

Within the cortex, neurons are organized in a highly structured manner depending on their function and receptive field properties. Hubel and Wiesel (1962, 1968) proposed the first known model of cortical hypercolumns (a modern view of hypercolumns is presented in Figure 5). A hypercolumn is a column of V1 neurons with similar spatial frequency (recall Figure 1) and position preferences covering the full range of orientations. The primary visual cortex is tesselated with hypercolumns covering the entire visual field.

1.1.4. Spatial Frequency Contrast Sensitivity

Campbell and Robson (1968) provided psychophysical evidence suggesting that the visual system decomposes retinal images into their Fourier components. They measured spatial frequency contrast sensitivity functions for different observers (specifying how much contrast the observer needed to detect certain spatial frequencies) using sine-wave gratings of various frequencies (see Figure 6). They showed that contrast sensitivity for patterns composed of sinusoidal luminance oscillations summed

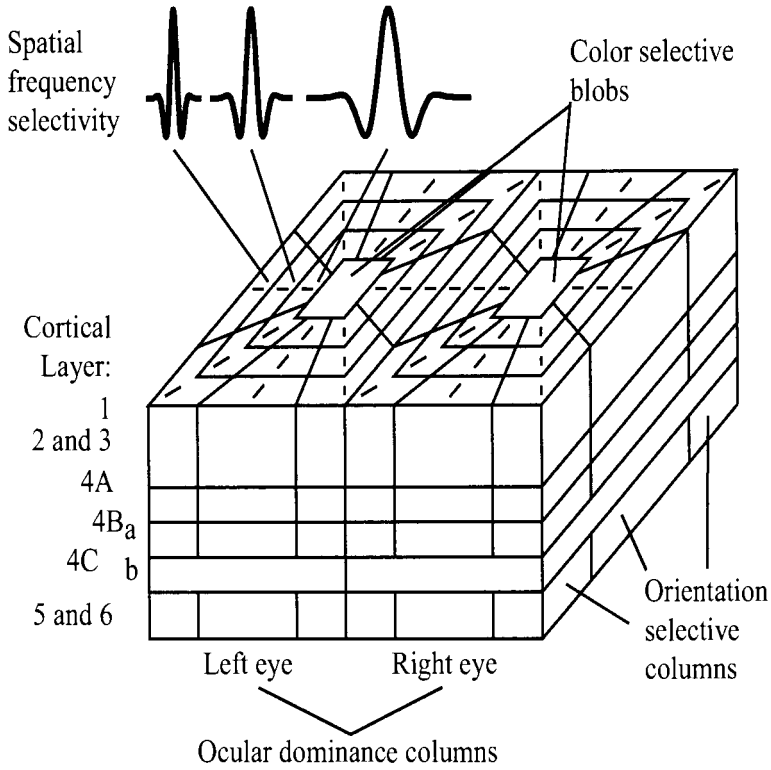

Figure 5. A hypercolumn. The primary visual cortex (V1) is subdivided into ocular dominance columns receiving input from the left and right eyes. At the center of each ocular dominance column is a color selective blob that is not tuned for contrast orientation. Within an ocular dominance column, orientation columns are selective for local contrast orientation. Color tuned blobs are selective for different colors within each column. Radiating outward from the blobs the cells are tuned to progressively higher spatial frequencies. A hypercolumn consists of a column of cells including cells sensitive to all orientations.

over discrete frequencies could be predicted based on a subject's contrast sensitivity to the individual sine waves composing the patterns. These results suggest that the combined action of the retina, LGN and V1 (and likely other areas) serve to perform a kind of local Fourier decomposition on the incoming retinal image stream.

1.2. Temporal Vision

Temporal vision research is concerned with how the visual system processes dynamically changing scenes. Similar to spatial vision, thousands of temporal vision papers have been published and this review will only cover a subset of the more

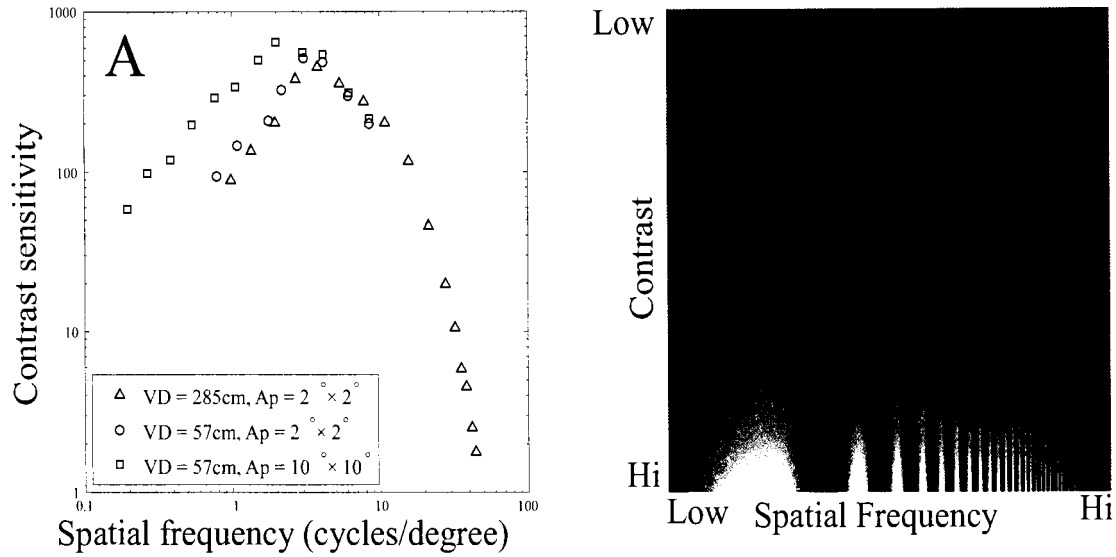

Figure 6. A: Spatial frequency - Contrast sensitivity functions obtained by Campbell and Robson (1968). Figure re-plotted based on their Figure 2. VD = Viewing Distance and Ap = viewing aperture size. B: In this plot spatial frequency increases from left to right while contrast increases from top to bottom. Different bars appear to end at different heights because of the observer's spatial frequency - contrast sensitivity function. The resultant border of visibility is similar to the functions obtained in A.

foundational and influential papers from the field. In particular, it will examine Hodgkin and Huxley (1952), Robson (1966), Albrecht et al. (2002), Lee and Blake (1999), Farid and Adelson (2001) and Blake and Lee (2005). Other more advanced papers that the reader might find interesting include Adelson and Bergen (1985) which deals with computational models of spatiotemporal processing, Buzsaki and Chrobak (1995) which deals with how neural ensembles may use synchrony to perform sensory binding and memory formation, Simoncelli and Heeger (1998) which elaborates on computational models for how V1 extracts contrast over space and time, Wilson (1999) which covers the basics of non-linear dynamical systems of equations and their application to modeling spiking neurons, Olshausen (2003) which outlines why V1's receptive fields are optimized for the natural environment and Izhikevich (2004) which provides simplified non-linear dynamical systems of equations for neural modeling while retaining biologically observable neural response properties.

1.2.1. Hodgkin and Huxley (1952)

In 1952, Hodgkin and Huxley measured voltage changes across the neural membrane of the Loligo (squid) giant axon and examined ion conductances associated with these voltage changes. They found that membrane potentials could be accurately modeled if characterized in terms of four electrical currents across the membrane (sodium, potassium, leakage and stimulating currents) as well as the membrane's capacitance. Using a non-linear dynamical system of four equations (one for each membrane current), each of whose parameters were derived from empirical observations, Hodgkin and Huxley were able to accurately reproduce neural spiking behavior in their model (Figure 7). Not only did this work win Hodgkin and Huxley the 1963 Nobel Prize in Physiology or Medicine, but these equations have provided the most accurate representation of neural firing available to date and have predicted results (such as chaotic behavior) that Hodgkin and Huxley had not imagined at the time they wrote their seminal paper. Their work spawned a cornucopia of subsequent papers and books that examined their model's properties and led to newer simplified models that retained the original model's key attributes but allowed for analytic analysis of the model's isoclines and bifurcations (Morris and Lecar, 1981; Hindmarsh and Rose, 1982, 1984; Rinzel, 1985; Rinzel and Ermentrout, 1989; Rose and Hindmarsh, 1989; Kepler et al., 1992; Rieke et al., 1997; Wilson, 1999; Izhikevich, 2004, 2006).

While the Hodgkin and Huxley (1952) model comprehensively accounted for individual neural functioning over time, it did not account explicitly for how networked neurons function over time. An open question, then, is how temporal sensitivity measured at the systemic/behavioral level arises from what is ultimately a collection of networked neurons. While the full answer to this question is not yet clear, some hints may be gained by examining the behavior that such neural networks yield. This is the next section's topic.

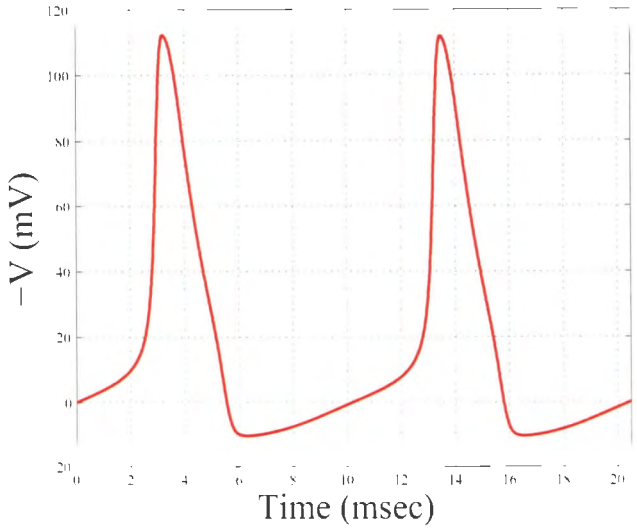

Figure 7. Example spikes produced by the Hodgkin and Huxley (1952) model. These spikes were produced with a constant input of 0.6 mV.

1.2.2. Robson (1966)

Robson (1966) examined the human temporal frequency contrast sensitivity function, which is a product of the action of many neurons acting collectively. He found that the visual system is differentially sensitive to different spatiotemporal frequencies. He measured contrast sensitivity over a full range of spatial frequencies at four different temporal frequencies (using flickering gratings) and observed the data reproduced in Figure 8. Here, subjects's contrast sensitivity was measured as both a function of spatial frequency and temporal frequency using drifting gratings. This data imply that the visual system is not uniformly sensitive to all temporal frequencies, but rather, that it has a certain range over which it is maximally sensitive and that sensitivity falls off quickly beyond this range. Furthermore, it suggests that spatial frequency and temporal frequency do not produce independent contrast sensitivity functions, but rather that they jointly influence contrast sensitivity.

Related studies using masking have found evidence suggesting that the observed contrast sensitivity functions are the outcome of the action of multiple frequency and orientation selective channels (Wilson, 1978; Wilson et al., 1983), suggesting that the

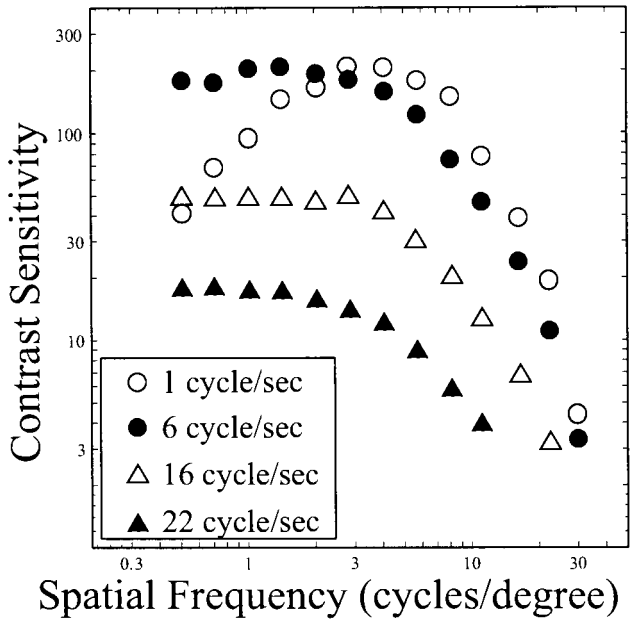

Figure 8. Human spatio-temporal contrast sensitivity function for a typical observer. Data re-plotted from Robson (1966).

visual system is performing a sort of Fourier decomposition of the retinal image.

1.2.3. Albrecht, Geisler, Frazor and Crane (2002)

In the studies described so far there is a conspicuous paucity of data relating to the neural contrast response function's temporal properties. This situation was remedied by Albrecht et al. (2002), who undertook a detailed examination of this issue. They characterized the temporal contrast response function for cat area 17 neurons and monkey V1 neurons. They found that these neurons exhibited local contrast-based response normalization and that this normalization was evident as early as 10 milliseconds following response onset. Furthermore, they found that V1 neurons integrate contrast over time following a Naka-Rushton type response integration profile. Figure 9 illustrates the full joint time-response to contrast function for a typical neuron. The main take-home message of this figure is that higher contrast leads to earlier neural responses and higher response rates. This is important because it means that not all neurons responding to a given scene will respond at the same

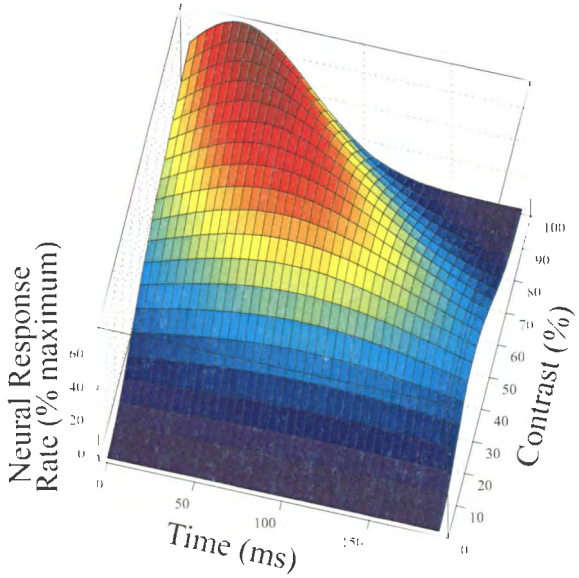

Figure 9. The temporal contrast response function as measured from cats and monkeys. A V1 neuron's post stimulus time histogram for a briefly presented Gabor (200 milliseconds) varies with both Gabor contrast and with time from stimulus onset.

time - a neuron's temporal response properties are dependent on local contrast.

1.2.4. Spatial Grouping Using Temporal Cues

Recently a heated debate has sprung up over how the visual system performs spatial grouping using temporal cues. The first article to really spark the flame in this debate was Lee and Blake (1999) (although papers that had already been published on the topic include Hogben and Di Lollo (1974). Rogers-Ramachandran and Ramachandran (1998) and Usher and Donnelly (1998)). Lee and Blake conducted an experiment where they had subjects view randomly oriented Gabor patches evenly distributed on a lattice filling an image. Each Gabor's carrier wave moved in a direction orthogonal to its orientation and the Gabors changed directions at random times. Lee and Blake (1999) defined a rectangular patch of Gabors as a figure and distinguished it from the background by making all of the figure Gabors change direction at the same time while the background Gabors each changed direction in an uncorrelated manner. The subjects' task was to identify the rectangle's orientation (vertical or horizontal) and task difficulty was varied by changing the rectangle's

aspect ratio. Here, the only information available to subjects for task performance was the temporal structure of the contrast changes. In spite of the paucity of available information, subjects were able to perform the task at above chance levels. Based on these results Lee and Blake (1999) argued that the visual system is performing local contrast detection through time and is correlating the times at which contrast changes occur over neighboring local elements, segmenting those elements over which sharp temporal contrast correlation boundaries exist and grouping those elements that share close temporal contrast correlations.

Subsequent to Lee and Blake (1999)'s paper Kandil and Fahle (2001) and Sekuler and Bennett (2001) wrote papers which lent further support to Lee and Blake (1999)'s argument replicating the finding that synchronized contrast changes can facilitate perceptual grouping and scene segmentation.

Following Lee and Blake (1999)'s discovery, Farid and Adelson (2001) demonstrated that Lee and Blake (1999)'s stimulus contained a transient temporal contrast cue that was detectable through temporal filtering that unambiguously yielded the rectangle's shape. Farid and Adelson (2001) conducted their own experiment using a stimulus containing randomly moving dots that was parameterized so that it could provide or be free of the type of transient temporal contrast cue present in Lee and Blake (1999)'s study. They found that subjects could accurately perform the rectangle orientation identification task when the temporal contrast cue was present but not when it was absent. Based on these results Farid and Adelson (2001) argued that "... synchrony is not responsible for the perception of form in these or earlier displays." Furthermore, they noted that blurring Lee and Blake (1999)'s stimulus produced transient spatial cues that could be used for task performance using single stimulus frames.

In a rebuttal to Farid and Adelson (2001), Blake and Lee (2005) created stimuli

for which blurring between the frames yielded no transient spatial cues for task performance and their data still showed that observers engaged in perceptual grouping and segmentation based on temporal structure. They also argued that they never implied anything other than that the visual system engages in temporal filtering and highlighted that the results of temporal filtering is enhanced contrast in the temporal domain, which is exactly where they were proposing synchrony detectors would operate. They also noted that it is the correlated dynamic fluctuations in temporal filter outputs that facilitate grouping and segmentation, not static patterns generated by the filtering process.

More than this, Blake and Lee (2005) compiled a summary of articles studying spatial segmentation based on temporal variations in luminance, contrast or contrast orientation. Interestingly, their summary highlighted a pattern of results suggesting that temporal modulations alone can promote perceptual grouping and segmentation, but that when these temporal modulations are paired with auxiliary cues such as orientation differences that promote the same pattern of perceptual grouping and segmentation, the temporal modulations have a relatively weaker effect. Similarly, when spatial and temporal cues are in conflict, the perceptual grouping and segmentation process typically favors spatial cues.

Furthermore, Rainville and Clarke (2008) recently conducted experiments where they stochastically modulated image elements over time along one of several potential dimensions, or messenger types, such as contrast, position, orientation or spatial scale to form vertical or horizontal rectangles. The subjects's task was to identify the rectangle's orientation based on the temporally modulated grouping cues. Crucially, they manipulated whether the task-relevant temporal-grouping information resided in the stimuli's carrier waves, the stimuli's envelope, or in the combined carrier and envelope of each messenger's timecourse. They found grouping to be messenger-

type specific in cases where the carriers contained grouping information but where the envelopes did not and grouping was messenger-non-specific in cases where the envelopes did contain grouping information. These results imply that temporal grouping may be mediated by messenger-specific carrier pathways and messenger-nonspecific envelope pathways.

1.3. Joint Spatiotemporal Vision

In order to fully understand the visual system, it is important to examine its responses to contrast changes over both space and time. This issue was touched on by Robson (1966), where he examined contrast sensitivity as a function of both spatial frequency and temporal frequency. Such studies reveal that the human spatiotemporal contrast sensitivity function can not simply be modeled as a product of individual spatial and temporal contrast sensitivity functions (i.e. the joint function is not a separable function of space and time). Furthermore, several neurophysiological experiments have found that a large number of V1 cells respond to drifting bars and edges, or drifting gratings (Hubel and Wiesel, 1962, 1968; De Valois et al., 1982), suggesting that V1 cells cover a spectrum of joint spatiotemporal frequencies. Sensitivity to a spatiotemporal frequency with non-zero x- and y-spatial frequency components implies that a cell has local-motion selectivity (Adelson and Bergen, 1985; Simoncelli and Heeger, 1998) and in cases where the x- and y-spatial frequency components are zero it implies flicker selectivity. Speed (s) and direction (θ) are related to spatiotemporal frequency by:

$$s = \frac{\omega_t}{\sqrt{\omega_x^2 + \omega_y^2}} \tag{1}$$

$$\theta = atan\left(\frac{\omega_y}{\omega_x}\right). \tag{2}$$

Here, ω_t denotes temporal frequency, while ω_x and ω_y denote spatial frequency in the

x- and y-directions. A given V1 simple cell, then, can be viewed as responding to motion at a given speed and direction over its spatiotemporal window of sensitivity. Simple cell responses to a drifting grating typically peak at a certain phase of the grating's drift cycle and fall off outside of this peak region (De Valois et al., 1982). This behavior is commonly known as phase-selectivity. Different simple cells' responses peak at different phases. Complex cells, on the other hand, generally show phase-invariance, meaning that they have high spike rates for all grating phases (De Valois et al., 1982). Complex cell responses to motion differ from those to flicker (see Figure 10). In response to motion, complex cells exhibit a sustained response, but in response to flicker they exhibit an oscillating response (De Valois et al., 1982).

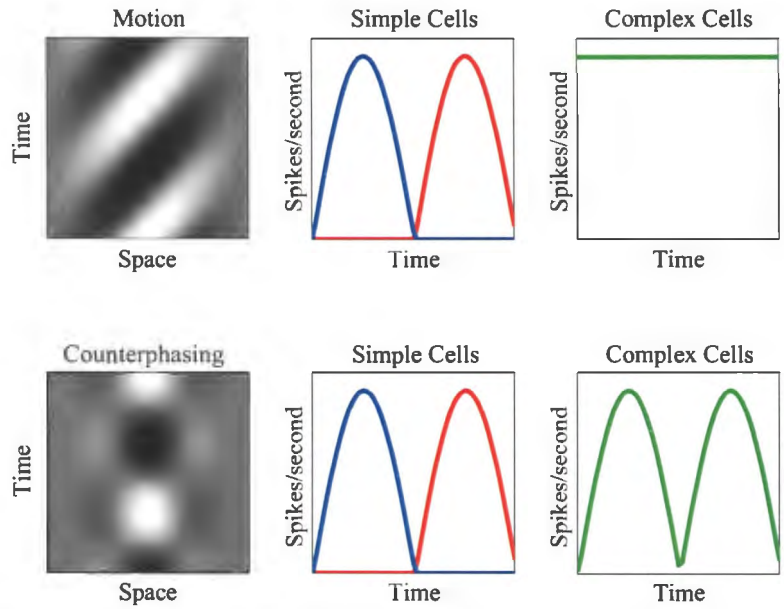

Figure 10. Simple and complex cell responses to moving (top row) and counterphasing (bottom row) gratings.

1.4. Pattern Vision

Pattern vision research is concerned with how the visual system integrates spatial and temporal information to detect patterns in the visual input. Pattern vision research is informed by both the spatial and temporal vision literature. Again,

literally thousands of pattern vision articles have been published and this review will only cover a subset of these that are foundational and influential.

1.4.1. Field, Hayes and Hess (1993)

Vision does not end with simple and complex cell responses. Following simple and complex cell response extraction, a series of operations are performed on V1 outputs that culminate in a person's conscious experience of the visual world. Although not every step involved in this process is known, several clues point to what the next step might be.

Field et al. (1993) performed experiments using primitive Gabor-like stimuli of the form known to elicit high firing rates from V1 neurons as evidenced by the experiments of De Valois et al. (1982). They provided psychophysical evidence suggesting that the visual system alters the salience of these image primitives based on spatial configuration. In particular, they found that contours made up of collinear and co-circular Gabor configurations were more detectable than contours made up of parallel or perpendicular Gabor configurations. This finding suggests that V1 neurons connect in a facilitative way with other V1 neurons whose receptive fields form collinear or co-circular relationships and in an antagonistic way with other V1 neurons whose receptive fields form parallel or perpendicular relationships. Thus, higher-level object representations may be built up from low-level image primitives by selectively grouping neurons with particular receptive field configurations. Field et al. (1993) called these collections of receptive fields "association fields" (Figure 11).

Later studies examining the statistics of natural images found that local edge elements on global object-bounding contours tend to pair with their neighboring edges in a way consistent with a local association field model (Kruger, 1998; Sigman et al., 2001; Geisler et al., 2001; Elder and Goldberg, 1998a, 2002). This suggests that the association fields evidenced in human vision may serve to help build up object

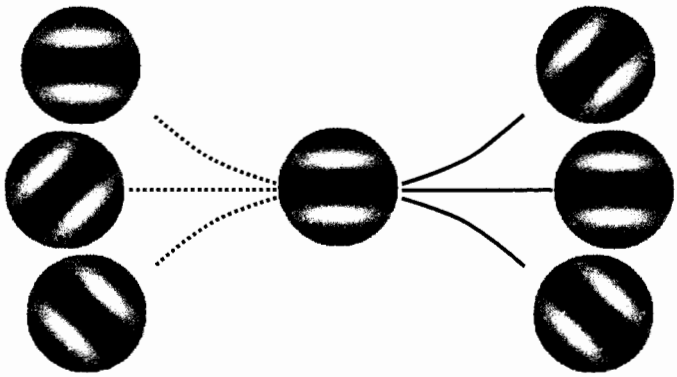

Figure 11. Association Field. Receptive fields that form parallel or perpendicular spatial relationships are unlikely to group together (denoted by dotted lines), while receptive fields that form collinear or co-circular spatial relationships are likely to group together (denoted by solid lines).

representations in an ecologically optimal way.

Association fields primarily exploit what the Gestalt psychologists of the 1920's and 1930's called proximity and good continuation (Köhler, 1920; Koffka, 1935; Wertheimer, 1938). More than these, however, the Gestalt psychologists provided behavioral evidence suggesting that the visual system also exploits similarity, symmetry, closure and common fate for perceptual grouping (see Figure 12). Proximity refers to how far apart two image features are. Good continuation refers to how smoothly image features vary in their orientations. Similarity refers to how close two image features are on dimensions like luminance, contrast polarity, shape, etc.. Symmetry refers to how well one side of an image maps onto the mirror reflection of the other side of the image (i.e. *mirror symmetry*) as well as to how well points in an image map on to other points reflected through the center of the image's coordinate system (i.e. *rotational symmetry*). These cues will become relevant in my Methods section where I use them to construct stimuli that elicit percepts of different numbers of objects in an image.

1.5. Modeling V1 Responses

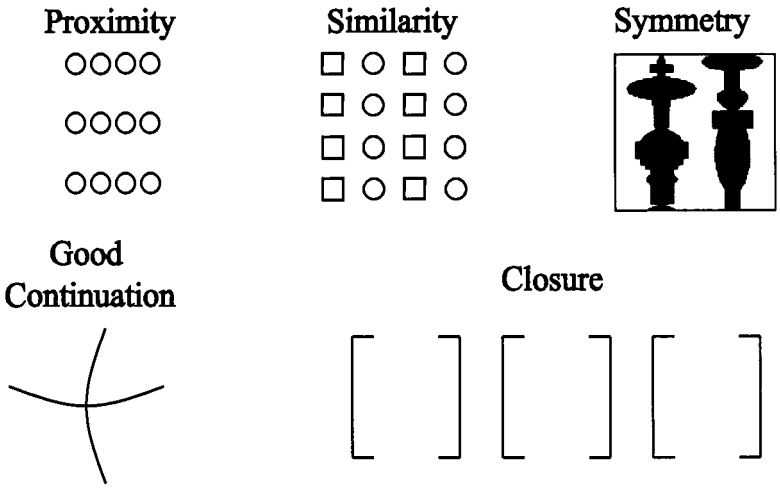

Figure 12. Gestalt grouping cues. Proximity: because the circles are closer together horizontally than they are vertically, they group into rows instead of columns. Similarity: because the elements in a column are similar, the elements group into columns instead of rows. Symmetry: because the black sections are symmetrical, the figure groups into two symmetrical black objects against a white background instead of three asymmetrical white objects against a black background. Good continuation: this figure groups into two smooth contours - one horizontal and one vertical as opposed to two pointed contours each touching at their cusp. Closure: this figure groups into closed squares instead of open "I" shapes.

In order to model the local Fourier decomposition imputed to be performed by V1, researchers have traditionally convolved the image with a set of wavelets like those depicted in Figure 4, but spanning a range of spatiotemporal frequencies in octave intervals, and spanning the full range of possible orientations (i.e. 0° to 360°) with two phases (0° and 90°) at each spatiotemporal frequency/orientation combination (Simoncelli and Heeger, 1998). The results of convolving an image with this type of filter bank yields model neural firing rates that can be negative and are unbounded (i.e. they can be infinite). Real neurons have positively valued firing rates and have a maximum firing rate beyond which they can fire no faster. In order to take these constraints into account, the convolution results are typically made positive through some form of rectification like half-wave rectification and squaring (i.e. half-squaring) and following this procedure, the convolution results within a given spatial region

are normalized (typically through divisive normalization, shunting inhibition or a winner-take-all scheme) (Heeger, 1992; Carandini et al., 1997). This procedure is depicted schematically in Figure 13 and yields simple cell responses that resemble those reported in physiological recordings by Hubel and Wiesel (1962) and De Valois et al. (1982).

In order to model complex cell responses, the V1 simple cell responses are typically summed over the two measured phases (0° and 90°). This produces neural responses that are selective for spatial frequency and orientation, but that are phase-invariant.

Similar to spatial vision, temporal vision is generally modeled using a local Fourier decomposition such as a wavelet code. Unlike spatial vision where a filter can be convolved with an image in either a forward or reverse direction, in temporal vision filtering may only include present and past information (future responses remain unknown). This constraint necessitates the use of *causal* filters - filters that use past and present but not future information (Figure 14).

In order to build up a temporal frequency selective neuron from spatial frequency selective neurons it has been hypothesized that the responses of a cascade of neurons all with the same spatial frequency selectivity are pooled over time with each neuron's input reaching the pooling cell with a slight temporal offset (see Figure 15) (Reichardt, 1969; Adelson and Bergen, 1985). In this way, a single set of spatial filters may be applied to an image and, depending on how they are connected to temporal pooling cells, they may combine to produce cells selective for different temporal frequencies. This mechanism may be used to confer motion selectivity to V1 simple cells, or, as in the example presented in Figure 15, flicker sensitivity.

Speed and direction, of course, are related to spatiotemporal frequency as outlined in Equations 1 and 2.

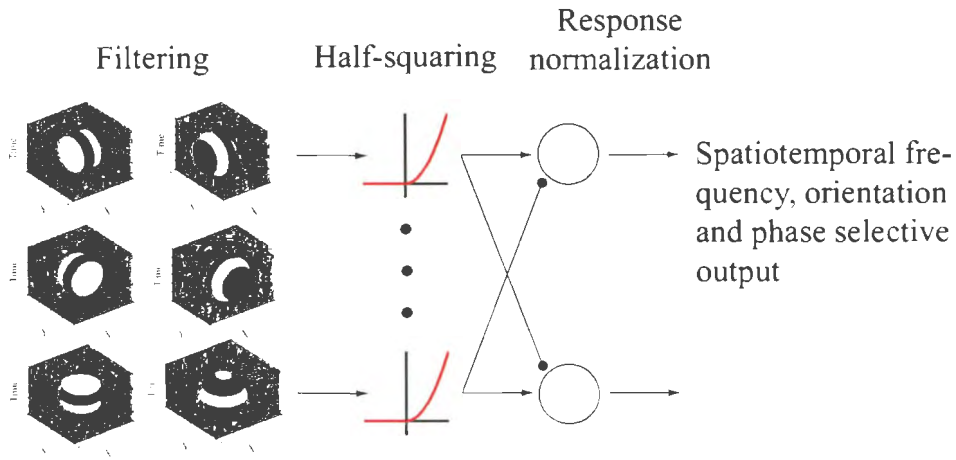

Figure 13. Schematic diagram illustrating V1 modeling. In the filtering stage a wavelet filter bank spanning multiple spatiotemporal frequencies, different orientations (different rows) and different phases (different columns) are convolved with the retinal image. In the half-squaring stage, the convolution results are half-wave rectified and squared. At the response normalization stage the activity in a local region is used to normalize the individual neural activity levels within that region. The outputs are selective for spatiotemporal frequency, orientation and phase, but consist of positive values bounded at an upper limit corresponding to the neuron's maximal firing rate.

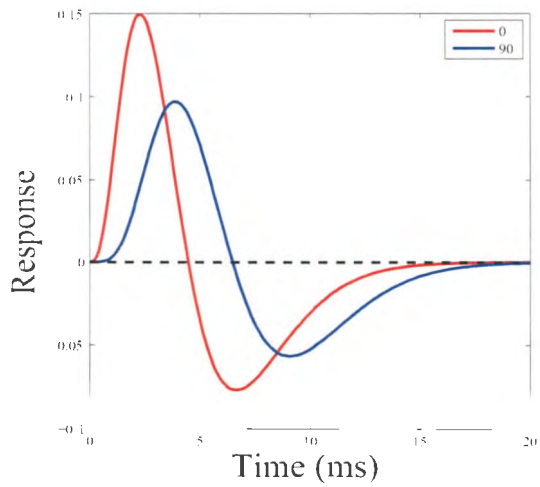

Figure 14. Two examples of causal filters used in modeling the temporal impulse response function of V1 neurons. Filters are in quadrature phase with the 0° phase filter marked in red and the 90° phase filter marked in blue. Note that filter responses are only defined in the positive temporal direction.

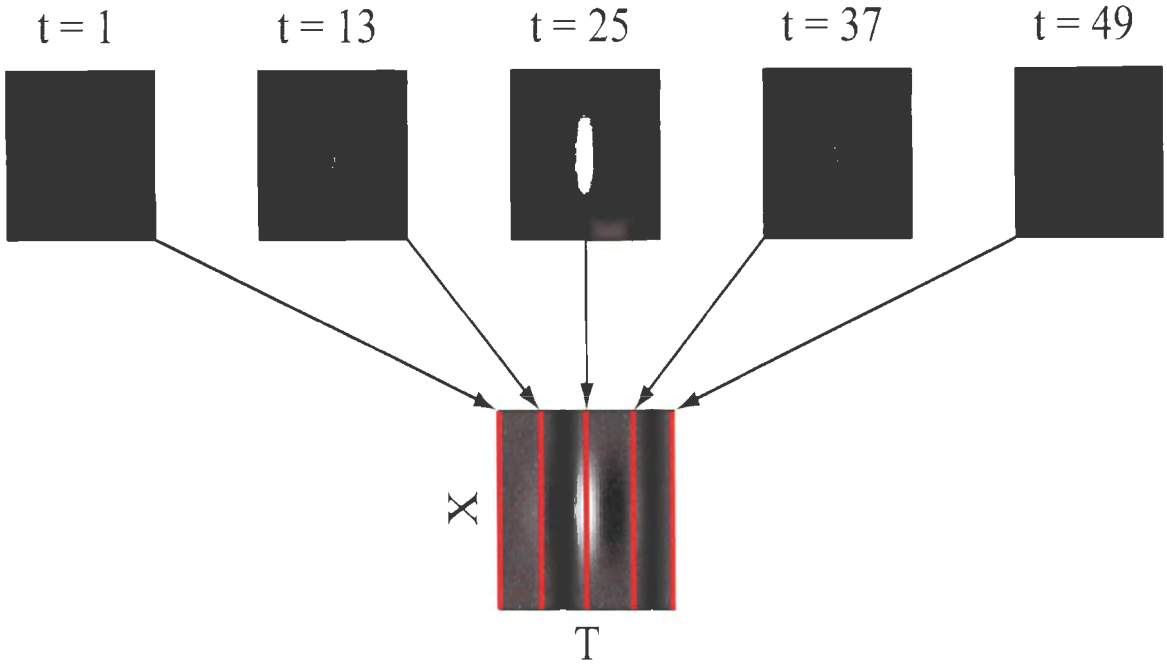

Figure 15. Temporal pooling. A neuron whose responses evolve over time can be constructed by summing the outputs of neurons sensitive to different inputs at different times. This neuron responds to a grating that is flickering through time without moving.

Complex cells have been hypothesized to sum squared-simple-cell responses in order to arrive at contrast-energy estimates within each spatiotemporal frequency band (Adelson and Bergen, 1985). One outcome of this process is that the resulting complex cell responses to motion differ from those to flicker. As illustrated in Figure 10, in response to motion, complex cells exhibit a sustained response, but in response to flicker they exhibit an oscillating response (De Valois et al., 1982). Presenting subjects with contrast-flickering stimuli, then, allows one to externally drive an oscillatory response from complex cells in the primary visual cortex. This is a useful property that I will leverage in both of my experiments.

At every step in the process outlined in Figure 13 there are several variables involved. At the filtering step one must consider what kind of filter best describes V1 simple cell response profiles (Gabors, log-Gabors, difference of Gaussians, derivative

of Gaussians, oriented difference of Gaussians, balanced Gabors, etc.), what range of spatiotemporal frequencies to use and how densely to sample the spatiotemporal frequency space (e.g. Wilson and Gelb, 1984 suggest that six spatial-frequency-tuned mechanisms suffice), and how densely to sample the orientation space. At the response rectification stage one must consider what non-linearity best describes V1 cell response rectification (e.g. half-wave rectification, squaring, half-squaring, etc.). At the response normalization stage one must consider how large a spatial extent to pool responses over, whether to divisively normalize, to use shunting inhibition or to use a winner-take-all model, what spatial frequencies to pool over and what orientations to pool over.

Although this challenge may seem daunting several notable researchers have risen to meet it. Among these are Adelson and Bergen (1985), Heeger (1987), Simoncelli and Heeger (1998), Blakeslee and McCourt (1999) and Cope et al. (2008).

1.6. Kanizsa Figures

Kanizsa (1976) provided a popular example of a figure that uses proximity, good continuation, similarity, symmetry, and closure to influence one's percept. Figure 16 illustrates an example of a Kanizsa square. Here, strategically placed Pac-Man shapes induce the percept of a square even though there are no luminance discontinuities along much of the square's border (Gold et al., 1999, 2000). Since the induced contour percepts are illusory they are typically referred to as *illusory contours* (IC).

Prior reverse-correlation studies have shown that humans use information along the illusory contour border to make discrimination decisions even when no task-relevant information is present at those borders (Gold et al., 1999, 2000). These findings suggest that illusory contour processing is implicit and automatic. A later study by Murray et al. (2002), however, found that illusory contour processing becomes more cognitive and effortful the more peripheral the stimulus presentation

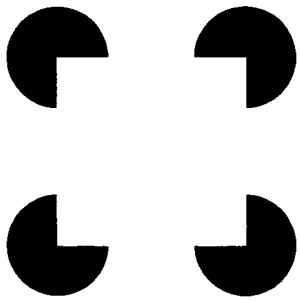

Figure 16. The Kanizsa square illusion (Kanizsa, 1976). Although no luminance discontinuities are actually present between the Pac-Man shaped symbols, subjects perceive edges at these locations, yielding the percept of a square.

and suggested different cortical pathways for the processing of foveal and peripheral illusory contours.

The determination of the cortical locus for illusory contour processing has been a topic of much debate in the scientific literature. Several studies have found activation as early as V1 (Hirsch et al., 1995; Mendola et al., 1999; Larsson et al., 1999; Seghier et al., 2000; Ohtani et al., 2002; Halgren et al., 2003) and V2 (Hirsch et al., 1995; Ffytche and Zeki, 1996; Goebel et al., 1998; Mendola et al., 1999; Larsson et al., 1999; Seghier et al., 2000; Ohtani et al., 2002; Halgren et al., 2003), however, several other studies have found no activation in either V1 (Goebel et al., 1998; Kruggel et al., 2001; Murray et al., 2002; Pegna et al., 2002; Brighina et al., 2003; Ritzl et al., 2003; Stanley and Rubin, 2003; Murray et al., 2004) or V2 (Kruggel et al., 2001; Murray et al., 2002; Pegna et al., 2002; Brighina et al., 2003; Ritzl et al., 2003; Stanley and Rubin, 2003; Murray et al., 2004) in response to illusory contours. Other areas that have been implicated in illusory contour processing include right Brodmann's area 18 (Hirsch et al., 1995), V5 (Goebel et al., 1998; Seghier et al., 2000; Kruggel et al., 2001) and the Lateral Occipital Complex (LOC) (Ffytche and Zeki, 1996; Mendola et al., 1999; Murray et al., 2002; Pegna et al., 2002; Halgren et al., 2003; Ritzl et al., 2003; Stanley and Rubin, 2003; Murray et al., 2004).

Studies examining the timing of illusory contour processing suggest that illusory

contours are initially generated in area LOC and, through a feedback cascade, elicit activity in earlier visual areas (Murray et al., 2002, 2004).

Several lines of evidence suggest that illusory contours are processed independently of contrast polarity (i.e. it does not matter if the inducers are black against a white background or if the inducers are white against a black background). Intracranial studies using macaques have revealed contrast-polarity-independent figure-ground responses (Baumann et al., 1997; Zhou et al., 2000; Peterhans and Heitger, 2001) as well as contrast-polarity-independence in responses to illusory contour presence versus absence (Heider et al., 2000). Behavioral studies have demonstrated that illusory-contour-percepts persist over variations in contrast polarity across inducers (Prazdny, 1983, 1986; Shapley and Gordon, 1985; Dresp and Grossberg, 1997; Victor and Conte, 1998; Spehar, 2000) and over variations in the induced shape's subjective brightness (Ware, 1981). fMRI studies have shown contrast-polarity-independence for illusory contour presence versus absence in area LOC (Mendola et al., 1999). Finally, VEP studies have shown contrast-polarity-independence for the timing of illusory contour processing (Murray et al., 2002).

Given the useful properties of Kanizsa squares and the robust nature of the square percepts they induce, these figures will form the principal stimulus for my second experiment.

1.7. Summary

Of relevance to the current research, the above literature review suggests that a contrast modulated Gabor patch will selectively activate one, or a small number of V1 cells in a localized region of the visual cortex, with simple cells being activated in a phase-locked manner to the incoming retinal image stream. With this piece of information in hand, one can next consider how best to use this property to probe synchrony's effects on V1 cell pairs. I will leverage this property of Gabor patches in

my first experiment and show that stimuli carefully constructed using Gabor patches may reveal information about how the visual system uses synchrony. In my second experiment, I will use Kanizsa squares and show that they too can reveal interesting information about how the visual system uses synchrony. The next chapter will expound on what synchrony generally means in the scientific literature, where its significance lies and what role synchrony plays in perceptual grouping and scene segmentation.

CHAPTER 2. SYNCHRONY

Synchrony refers to the simultaneous occurrence of two or more events in time. Neurally, synchrony occurs at multiple levels. Synchrony can occur at the single-spike level and at the spike-rate level (although these two levels become the same if one makes the latter's temporal integration window equal to a single spike's duration). Synchrony can also occur between two neural populations. Neural synchrony is ubiquitous in the brain (Engel et al., 1991a; Gray et al., 1989; Fries et al., 2001; Roelfsema et al., 1997; Steinmetz et al., 2000; Singer, 2004; Kreiter and Singer, 1996), the question of relevance pertains to its functional significance. Researchers have found evidence that neural synchrony is associated with perceptual grouping (Engel et al., 1991a; Gray et al., 1989), attention (Fries et al., 2001; Roelfsema et al., 1997; Steinmetz et al., 2000), coordinating information transmission between cortical areas (Engel et al., 1991c; Roelfsema et al., 1997) and even conscious awareness of events (Singer, 2004). Others, however, posit that neural synchrony results purely from neural responses phase locking to externally synchronous stimuli - like a boat rocking back and forth in response to the waves - or from chance resonance within the cortical circuitry, where the brain doesn't actually care that its neurons are responding synchronously and makes no use of that synchrony for internal functioning (Shalden and Movshon, 1999). They caution that the current body of experimental evidence does not warrant claims for neural synchrony's functional role in the cortex, that the computational complexity required of individual neurons in order to use synchrony is unreasonable and that alternative mechanisms exist for performing the tasks that have been attributed to neural synchrony (Shalden and Movshon, 1999). In this document I shall review the evidence bearing on neural synchrony's role in cortical processing, I will conduct an experiment that clears up some questions about synchrony's importance and I will propose a computational model that explains my

experimental results.

2.1. Synchrony Sources

One point of general agreement in the scientific community is that synchrony does occur in the brain. In binocular rivalry experiments, for example, Fries et al. (1997) found that all stimulated neurons responded with a high firing rate, but that the rivalrous neurons winning the competition had relatively more synchronous responses than the neurons losing the competition (as measured by spike-field coherence). Engel et al. (1991c) showed that synchronization between different cortical hypercolumns may be observed in the cross-correlograms performed on neural spike trains when the stimulated hypercolumns were responding to parts of the same object. Engel et al. (1991c) also showed through cross-correlation analysis on unit responses that cat area 17 neurons can synchronize with neurons in the cat's posteromedial lateral suprasylvian area. Engel et al. (1991a) found that neural pairs in cat area 17 can even synchronize across hemispheres (as evidenced through cross correlograms performed on neural spike trains) and that this synchronization was abolished by sectioning of the corpus callosum, suggesting that the observed synchronization was resultant from cortico-cortical connections.

Starting with this point of agreement then, in this section I shall examine when and how neural synchrony occurs in the brain. This, in turn, shall yield some hints as to neural synchrony's functional importance.

Synchronous neural firing may arise from at least three possible sources:

1. Stimulus-locking: Different neurons responding to the same stimulus will fire at the same time when the stimulus changes (Singer, 2004).

2. Common input: Different neurons that receive their inputs from a common upstream "parent" neuron will both fire when stimulated by their common parent

(Singer, 2004).

3. Dynamic interactions within the cortical network: some neurons fire transiently in synchrony when the cortical network is in a particular state and stop firing synchronously when the network state changes (Singer, 2004). This is analogous to how a section of violinists will all play in unison during one part of a concerto but will start playing different tunes at a different part of the concerto. Their synchrony depends on the state of the concerto. Hutcheon and Yarom (2000) suggest that this category may be subdivided into three subordinate categories based on the neuron's state of resonance and amplification: (a) synchrony caused by resonance alone; (b) synchrony caused by weak interactions between resonance and amplification; and (c) synchrony caused by strong interactions between resonance and amplification that can destabilize a neuron's resting membrane potential and induce it to become spontaneously oscillatory.

Each of these synchrony sources is important in its own right. Although the bulk of this paper shall focus on dynamic interactions within cortical networks, interesting insights may be gained by examining the first two synchrony sources in a little more detail.

2.2. Stimulus-Locking

Stimulus-locked synchronous responses have been found in many different areas throughout the brain. Rager and Singer (1998), for example found that flickering visual stimuli manifest as well-synchronized cortical responses, indicating that relative spike timing is preserved when transmitted from the retina through the LGN to the cortex. Other experiments (Castelo-Branco et al., 1999) and modeling studies (Stevens and Zador, 1998) have revealed that relative spike timing is reliably transmitted with a precision in the millisecond range and that oscillatory retinal responses

are reliably and retinotopically transmitted to the cortex. With every biological operation there is an associated cost. In the case of neural firing, for instance, there is a high metabolic cost. Less than one percent of cortical neurons can be concurrently substantially active (Lennie, 2003). Given this high cost, there is a strong evolutionary drive to reduce the number of substantially active neurons involved in cortical computations. Only important computations are allowed to proceed and they must do so in the most efficient way possible. Despite some temporal variability in neural responses to stimuli, some have argued that neurons have sufficient fidelity to carry important information in their spike timing. It is thus likely the case that synchronized neural signals carry some useful information, especially since firing two neurons at the same time uses more metabolic resources per unit time than would be used if their firing were spread out in time or if only one neuron were to fire. The results of several experiments showing that temporal synchrony in a stimulus can facilitate spatial grouping (Elliott and Müller, 1998; Fahle, 1993; Lee and Blake, 2001; Parton et al., 2001; Usher and Donnelly, 1998; Koepsell et al., 2010) suggest that the useful signal carried by stimulus-locked neural synchrony is a perceptual grouping cue. Specifically, when an object's image projects onto the retina, all of its local parts project images that change at the same time or at very close times (i.e. they change along a smooth temporal gradient). The neurons responding to the object's parts become active at the same time and these synchronous responses indicate that the responding neurons represent information that should be grouped together. Imagine viewing a moth camouflaged against a tree trunk. As long as the moth remains still it is difficult to distinguish from its surrounds, but as soon as it moves, all of the neurons responding to its image begin to signal motion at the same time. A visual system that uses this exogenous synchrony cue presumably does a better job at correctly grouping and segmenting a retinal image than one that does

not use this cue.

2.3. Common Neural Input

Unlike stimulus-locking, synchrony from common input does not necessarily require the neural responses to be phase-locked to an exogenous stimulus. It only requires neural responses to be phase-locked with each other.

Within the brain one can find connections of all sorts - some neurons send their signals to many other neurons and some neurons send their signals to only one neuron. Similarly, some neurons receive signals from many neurons and some neurons receive signals from only one neuron. A neuron that sends its message to many others may cause neural synchrony among the neurons it connects to. This is useful for the same reason that stimulus-locking is useful - if information about the same object is being sent to two cortical areas then the temporal grouping cues related to that object will need to be passed on to both areas in a reliable way in order for those cues to be maximally useful. What better way to reliably transmit the same temporal information than to have the same neuron seed activation in both cortical areas?

2.4. Synchrony From Dynamic Interactions Within The Cortical Network

Synchrony resulting from dynamic interactions within the cortical network does not have as easy an explanation as synchrony resulting from stimulus-locking or common input, but it happens often and in many different cerebral structures (for reviews see Engel et al. (2001) and Singer (1999)). To get a sense of whether or not this kind of synchrony has any purpose, lets examine the conditions under which it has been observed. Engel et al. (1991a) and Gray et al. (1989) found that the spatiotemporal patterning of synchrony resulting from dynamic cortical interactions depends on stimulus configuration. Cortical network activation state (meaning which neurons are actively firing and which neurons are silent) also seems to play a role

in determining the spatiotemporal patterning of synchrony resulting from dynamic cortical interactions (Herculano-Houzel et al., 1999; Munk et al., 1996), as does attention (Fries et al., 2001; Roelfsema et al., 1997; Steinmetz et al., 2000). For the time being, however, I will focus on the effects of stimulus configuration on neural synchrony.

In stimulus configuration experiments, researchers have presented animals with primitive stimulus elements like bars, edges and Gabor patches and have recorded from groups of two or more neurons in the thalamus or the primary visual cortex. Here, the typical finding is that neurons in different cortical hypercolumns (recall Figure 5) and in the same or different cortical areas and in the same or different hemispheres tend to synchronize their responses when stimulated with elements falling on a common contour and tend fire independently when stimulated with separate contours (Engel et al., 1991a,b,c; Freiwald et al., 1995; Gray et al., 1989). Note that this is not the same as synchrony from common input because if the neurons were synchronizing based on a common input then the neurons that were not part of the same contour would synchronize by virtue of the fact that they were presented with their stimuli at the same time. At the receptive field level, synchrony tends to arise in both neurons with overlapping receptive fields and in neurons with non-overlapping receptive fields. However, for the neurons with non-overlapping receptive fields synchrony tends to arise only in those neurons with similar orientation preferences. These findings suggest that neurons whose receptive fields have a collinear or co-circular spatial arrangement (Field et al., 1993) are hard-wired to synchronize while those whose receptive fields form orthogonal spatial relationships are hard-wired to desynchronize (Yen et al., 1999).

Synchrony is not solely used to indicate that two neuron's local receptive fields lie on the same global object contour. At the surface perception level, analysis of

neural pair in areas 18 and the posteromedial lateral suprasylvian complex (PMLS) of cats reveals that they synchronize their activity if the contours they're responding to are perceived as belonging to a common surface (Castelo-Branco et al., 2000). In the medial temporal cortex (area MT), Kreiter and Singer (1996) found that MT cells in macaques with overlapping receptive fields, but with different motion direction preferences, can engage in synchronous activity when stimulated with a single moving bar, but when activated by two different bars, each moving in the direction preferred by the cells at the two respective sites, responses show no or far fewer synchronous periods. Whatever neural synchrony is observed while the bar remains unperturbed must be the result of some internal process for which it is useful to make neurons responding to a common bar fire at the same time.

Lisman (1996) argues that objects are neurally coded by synchronous bursts of activity. This implies that different objects could be represented cortically by synchronous neural bursts at different times, but all neurons responding to the same object would respond at the same time (von der Malsburg, 1981; Izhikevich, 2004). Lamme and Spekreijse (1998) conducted experiments whose results suggest that this may not be true of objects defined by texture, however, methodological problems with their experiment (i.e. they recorded from multiple neurons at the same time instead of from individual neurons) that were pointed out by Gray (1999) suggest that their conclusions may have been premature and that synchrony may still be involved with texture-based image segmentation.

Inspired by the existent body of literature citing a significant role for synchrony in defining object membership, Koepsell et al. (2010) implemented an image segmentation algorithm that encoded information about homogeneous image segments through different oscillation phases. Their algorithm captured contrast information in spike rates and image segmentation information in the phases of the spike trains.

Their results yielded natural scene segmentations that were qualitatively similar to human segmentations.

Fries et al. (1997) performed a binocular rivalry experiment where they recorded from cat area 17 neurons responding to both suppressed and un-suppressed eyes and examined the resultant firing patterns. They found that all stimulated neurons responded at a high rate, but more importantly that the neurons winning the competition had relatively more synchronous responses (as assessed through a neural response cross-correlation histogram) than the neurons losing the competition. The dominant synchronous responses had power in the gamma frequency range (i.e. 25 to 100 Hz).

More than generally eliciting power over the broad band of frequencies in the gamma range, however, Izhikevich et al. (2003) showed that neurons can selectively target which of the many neurons they synapse with for activation by changing their output spike frequency (while still firing within the 25 to 100 Hz range). Individual neurons are optimally stimulated by different input frequencies, so changing one's output frequency allows a neuron to specify which neuron to optimally stimulate even though that neuron might make connections with several other neurons (Izhikevich et al., 2003).

Neural synchrony's utility stretches even further than this, however, as within populations of synchronously oscillating neurons, individual cells can skip cycles (Buzsaki, 1996; Buzsaki and Chrobak, 1995), and neurons engaged in population oscillations of different frequencies can have partial correlations (Jensen and Lisman, 1998). These properties can be used to represent gradients and nested relations (Luck and Vogel, 1997).

2.5. Neural Oscillations

An oscillation is a periodic fluctuation in a given measurement over time. Neurons maintain electrical potentials over their membranes. These potentials may oscillate given the right conditions. Furthermore, neurons fire spikes. The rate at which neurons spike may also oscillate over time.

More than asking how synchrony arises, one might ask how neurons come to oscillate in the first place? Neural oscillations are an important prerequisite for neural synchrony and the mechanisms by which neural oscillations occur deserve some attention.

Hutcheon and Yarom (2000) posit that *resonance* and *amplification* are important factors involved in neural oscillations. Resonance refers to the ability of some neurons to respond selectively to stimulation by neurons oscillating in their firing (or membrane potential) at a particular frequency while amplification refers to the ability to increase responses over all input frequencies. A neuron that prefers 40 Hz stimulation, for example, will yield the highest response when stimulated with oscillatory inputs at 40 Hz and will respond less to oscillatory inputs of any other frequency. Subthreshold oscillations in membrane potential can be self-sustaining given the appropriate amplification.

Put together, these two neural properties (resonance and amplification) allow for three main forms of oscillation. The first is pure resonance where a neuron fires at a particular frequency under constant stimulation by another neuron. The second is an interaction between resonance and amplification where a neuron fires with a sustained oscillatory firing pattern at a given frequency if given the appropriate transient input. The third, and final oscillation type results from amplification that is so strong that it moves subthreshold membrane potential oscillations to the range where they can initiate action potentials and cause the neuron to engage in spontaneous and sustained

oscillatory firing.

2.6. Synchrony at the Behavioral Level

Although the effects of synchronous visual stimuli on *neural responses* have been shown to depend on the stimuli's spatial configuration, synchronous stimuli have also been shown to affect *behavioral responses* in a way that depends on spatial configuration. Figure 17 A and B show two stimuli that differ in their spatial configuration. Figure 17A shows a stimulus array where all of the elements are randomly oriented. This configuration yields no particularly salient percepts of any objects. Figure 17B, however, shows a stimulus array where the elements along the horizontal meridian are all collinear with each other and yield the percept of a single horizontal contour. Similar stimuli have been shown in single cell recording experiments to yield synchronous oscillatory responses from neurons whose receptive fields fall along the contour (Engel et al., 1991a,b,c; Freiwald et al., 1995; Gray et al., 1989; Kreiter and Singer, 1996). Recently, Cheadle et al. (2008) conducted a clever experiment using these two stimuli that revealed interesting behavioral effects related to synchrony between individual elements in these two stimulus configurations. Unlike prior experiments that used synchrony as a grouping cue to allow subjects to group or segment elements in a given image, Cheadle et al. (2008) used spatial configuration as the grouping cue and examined how different spatial configurations influenced a subject's synchrony percepts. In order to do this they made the two red and blue circled elements in 17A and B undergo square-wave oscillations in their contrast while the remaining elements were held fixed at 100% contrast. The contrast oscillating elements could oscillate either in phase or could oscillate with some arbitrary temporal phase difference. Given a set of contrast oscillating elements embedded in a given static background (a zero-objects randomly oriented background or a single-object horizontal line background) the subjects were asked to perform a two-interval forced-

choice task where they identified the interval containing the more synchronously oscillating elements. From trial to trial task difficulty was adjusted by making the elements in the two intervals more or less similar in their synchrony level. Critically, for a given synchrony level subjects' response accuracy varied depending on whether or not the oscillating Gabors were or were not part of a common contour (i.e. accuracy for 17A differed from accuracy for 17B). In particular, they found that subjects were able to make accurate synchrony discriminations over a smaller portion of the possible phase difference spectrum when stimulus elements formed a collinear contour than when they formed an orientation jittered pattern. This is consistent with a model where flickering elements on a zero-objects pattern (Figure 17A) are perceived veridically, but where flickering elements on a common contour (Figure 17B) are perceived as being more synchronous than they really are, resulting in a compression of the range of perceived synchrony levels and poorer performance on Cheadle et al.'s task. Cheadle et al. (2008) provide a model that describes behavioral performance on this task. This model is described in detail in the Modeling section, however, I shall outline a few key points here. Firstly, their model is premised on the notion that somewhere in the brain stimulus contrast oscillations are veridically transduced (although they do not specify whether these contrast oscillations are transduced into oscillations in membrane potentials, spike rates or population activity). This is not an unreasonable assumption given prior neurophysiological findings, however, it would have been preferable if they were explicit about what kind of oscillations they were talking about. Next, they posit that these internal oscillations are actively modulated by internal mechanisms that are sensitive to stimulus spatial configuration. The key predictions of the model are that the internal representations of the two oscillating Gabors are extended in time to have periods of overlapping high responses in the case where they fall on a common contour (the one-object pattern) and are represented

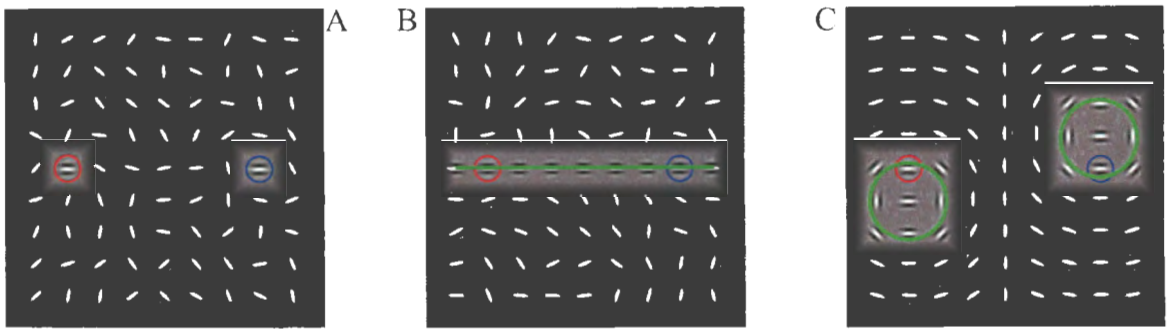

Figure 17. Example psychophysical stimuli. A: Zero-objects stimuli. B: One-object stimulus. C: Two-objects stimuli (object locations are marked in green). In each stimulus the two Gabors outlined in red and blue oscillated in their contrast while the remaining Gabors where held fixed at 100% contrast. The phase difference between red and blue Gabor oscillations varied from trial to trial. None of the red, blue or green marks appeared in the experiments conducted.

veridically where they fall in the randomly oriented array (the zero-objects pattern).

Yen et al. (1999) provide a black-box style model (i.e. a model with no specified neural dynamics) for how synchrony could be used to group neural responses stemming from a common object and segregate these from neural responses stemming from separate objects. Crucial to the formulation of Yen et al. (1999), however, is that responses to separate objects be actively *desynchronized*. This is important because if two neurons oscillating in response to separate objects happened to have similar starting phases, then they could end up being grouped together by chance even though they really belonged to separate objects. Active desynchronization avoids this problem because the neural oscillation phases representing separate objects are pushed apart even if they start off being similar. Cheadle et al. (2008) did not test for behavioral evidence of this phenomenon. Furthermore, the model they provide to account for their results, while producing the desired synchrony or lack-there-of, is not a biophysical model, does not relate to spiking neurons and fails to explain the canonical gamma frequency power observed in single cell recording studies and EEG paradigms that examine neural behavior under conditions of perceptual grouping. Similarly, Yen, Menschik, and Finkel's model, while describing some neural behavior,

is also not a biophysical model and has no explicit dynamical formulation.

In this dissertation I will provide behavioral evidence for active desynchronization between neurons responding to elements on separate objects and will develop a biophysical neural model that not only predicts my behavioral results, but which also explains the gamma frequency power observed in single cell recording studies and EEG paradigms that examine neural behavior under conditions of perceptual grouping.

CHAPTER 3. MODELING

In this Chapter I present two models that describe how synchrony can arise in the brain. The first is the Cheadle et al. (2008) model, which does not have an explicit level of description, but which may vaguely be interpreted as describing changes in membrane potentials, changes in the firing rates of individual neurons, or changes in the population activity of neural populations. The second model is based on Hodgkin and Huxley (1952)'s equations describing how neural membrane potentials change as a function of the ion currents traversing the membrane. In this model I network the neurons such that synchrony and asynchrony arise between neural pairs as asymptotically stable steady states depending on the input synchrony and on the neural coupling coefficients.

For each model I will provide a detailed description of how the model works and what it predicts for various inputs.

3.1. Cheadle et al. (2008)

The Cheadle et al. (2008) model produces results like those shown in Figure 18. They showed that their model is capable of producing behavior that is uncoupled or synchronously coupled and I show that it is also capable of producing behavior that is asynchronously coupled. Critically, however, their model is not a biophysical model and it does not predict the gamma range power that has been observed in electrophysiological studies of perceptual grouping (e.g. Fries et al., 1997). Furthermore, rather than imposing true phase-alignment in the signal's Fourier components, Cheadle et al.'s model simply has each responding neuron cause an increase in the responses of its neighboring neuron. This model, thereby changes neuron one and two's relative amplitudes depending on whether synchrony or asynchrony is desired, but does not directly manipulate phase (Goodell and Rainville, 2009).

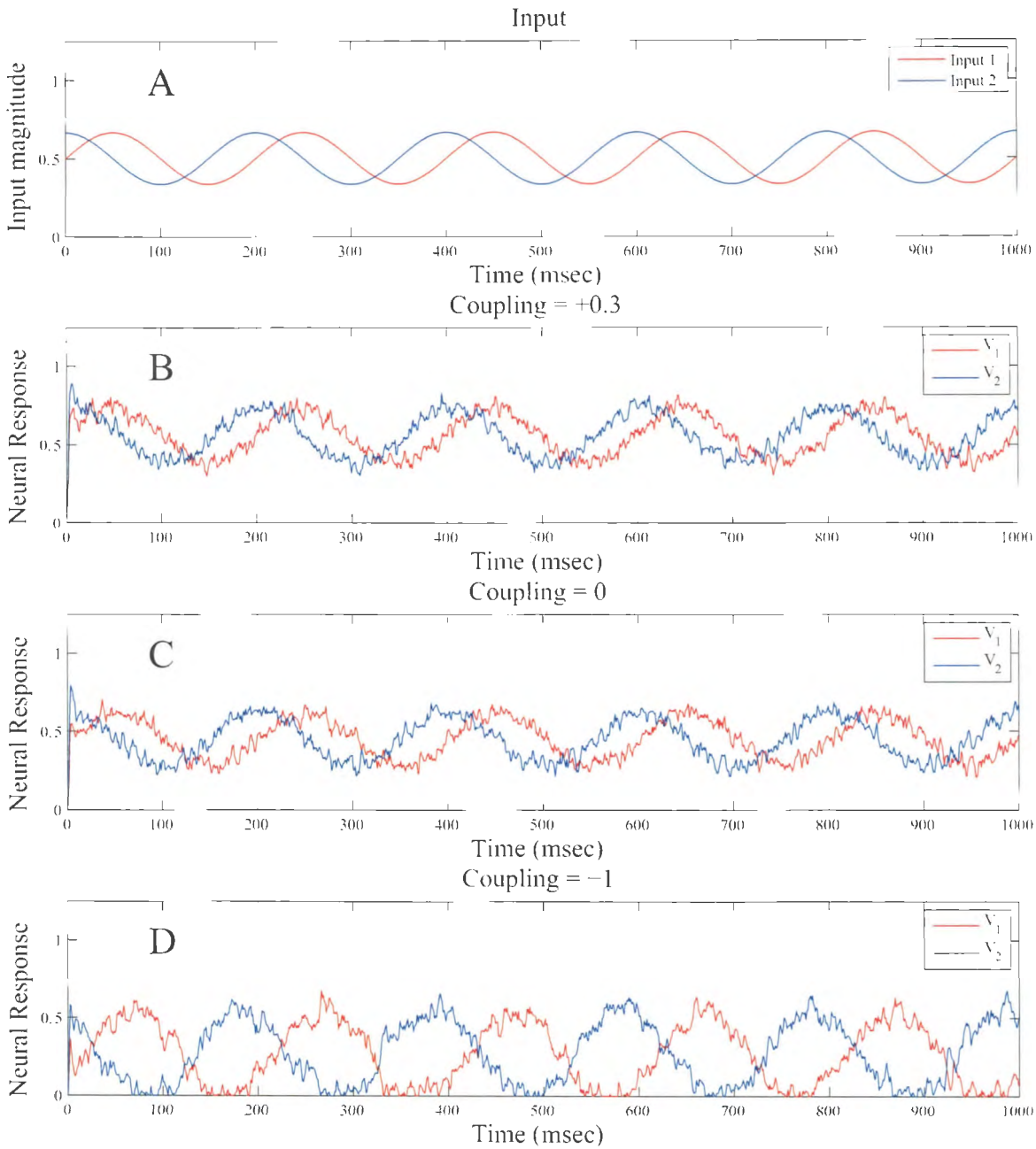

Figure 18. Simulation of Cheadle et al. (2008) with inputs shown in A using excitatory coupling shown in B, no coupling shown in C and inhibitory coupling shown in D (where D was not originally reported by Cheadle et al., 2008). Red traces denote inputs to and responses from V_1 while blue traces denote inputs to and responses from V_2 (see Figure 19). Abscissa plots time in milliseconds while ordinate plots input (A) and neural responses (B - D) in units that were unspecified by Cheadle et al. (2008).

Cheadle et al.'s model employs four neurons and is illustrated in Figure 19. Two neurons, V_1 and V_2, receive excitatory stimulus input and provide the main responses of interest. Connected to each of these two neurons are two more neurons, R_1 and R_2, that receive excitatory input from V_1 and V_2 respectively and provide inhibitory feedback. Additionally, each neuron has recurrent connections, V_1 and V_2 providing self-excitation (balancing the inhibition from the inhibitory neurons) and R_1 and R_2 providing self-inhibition (balancing the excitation from the excitatory neurons). Finally, V_1 and V_2 are coupled via mutual excitatory connections. The equations describing the neuron's behavior with respect to time (derived from Cheadle et al. (2008)'s discrete difference equations) are:

$$\frac{dV_1}{dt} = (1-k)[-V_1 + A_1F(V_1) - BF(R_1) + A_2F(V_2) + I_1 + noise](t) \quad (3)$$

$$\frac{dR_1}{dt} = (1-k)[-R_1 + CF(V_1) - DF(R_1)](t) \quad (4)$$

$$\frac{dV_2}{dt} = (1-k)[-V_2 + A_1F(V_2) - BF(R_2) + A_2F(V_1) + I_2 + noise](t) \quad (5)$$

$$\frac{dR_2}{dt} = (1-k)[-R_2 + CF(V_2) - DF(R_2)](t) \quad (6)$$

where t denotes time (ranging from 0 to 2000 msec in steps of 1 msec) k is a leaky integration constant (set to 0.98), A_1 is the self-coupling coefficient that determines the level of V-cell self-excitation (set to 1), A_2 is the coupling between V-cells (set to 0 for no-coupling and 0.3 for coupling producing synchrony), F is a firing rate nonlinearity which they specify as $F(x) = x/(1+x)$ for $x > 0$ and $F(x) = 0$ for $x < 0$ (this is a limiting case of the Naka-Rushton function with accelerating outputs for low input values and asymptoting outputs for high input values), B determines the inhibitory strength for the connection running from R to V (set to 1.75), C determines the excitatory strength for the connection running from V to R (set to

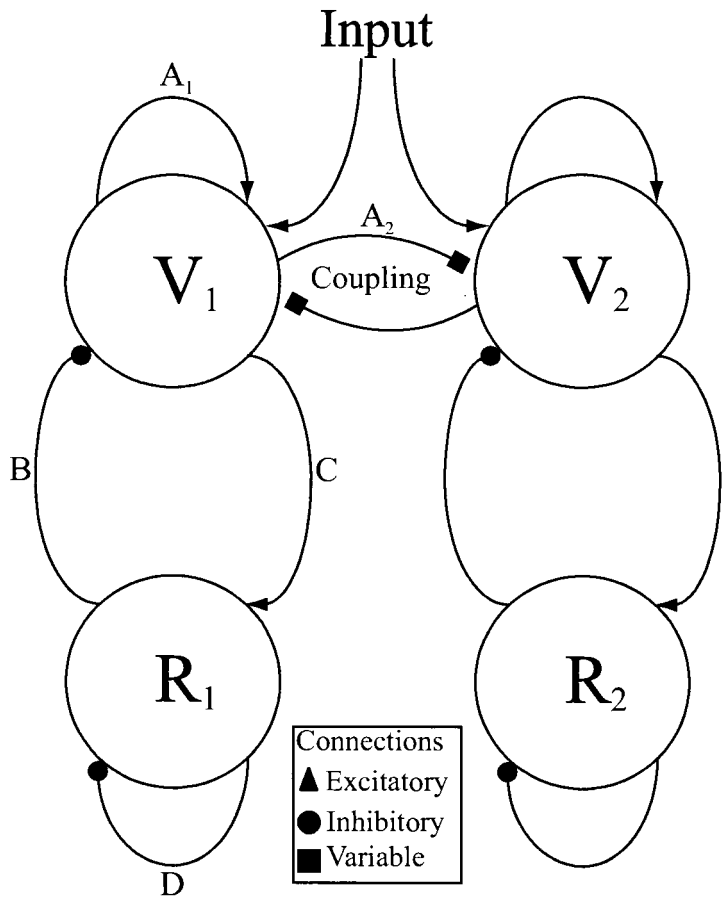

Figure 19. Schematic demonstrating networking between neurons in Cheadle et al. (2008)'s model. Arrows indicate excitatory connecitons, filled circles indicate inhibitory connections and squares indicate connections that may be either excitatory or inhibitory. V_1 and V_2 are excitatory neurons and R_1 and R_2 are inhibitory.

0.9), D determines the strength of self-inhibition on the R-cells (set to 0.1), noise is a variable sampled independently from a Gaussian distribution at each time point with a mean of zero and a standard deviation of SD_1 (set to 1), and I is the stimulus input (set to range between 0 and 0.33).

In Cheadle et al.'s original formulation their stimuli underwent square-wave contrast oscillations (not sinusoidal as shown in Figure 18A) and they manipulated stimulus synchrony by shifting the square-wave onsets for the two circled Gabors in Figure 17A and B by 0%, 25%, 50%, 75% or 100% of the square-wave's half-period - the maximal shift putting the inputs in anti-phase. To model human performance

using their equations they took these square-wave contrast oscillations as the inputs to their model's V-cells over time and calculated the level of asynchrony as the normalized signal difference between the two V-cells' outputs:

$$\frac{\int |F(V_1) - F(V_2)|dt}{\int |F(V_1) + F(V_2)|dt}. \tag{7}$$

Curiously, their normalization does not constrain the range of integrated response differences to a bounded region (such as [0, 1]). In order to relate this measure to subject's behaviors then, Cheadle et al. adopted the rule that if the amount of signal difference exceeded a given criterion threshold then they classified their V-cell outputs as asynchronous, otherwise the outputs were classified as synchronous. In order to model decision noise in the subjects' classifications, a second Gaussian noise term was added to the difference calculations prior to thresholding and classification. This noise term had a mean of zero and a standard deviation of SD_2, which was set to 0.25. This procedure allowed Cheadle et al. (2008) to generate psychometric functions for a two-interval forced-choice task using their model outputs instead of subject responses in order to predict how the subjects might respond to their task if the subject's neural mechanisms were actually implementing something like Cheadle et al.'s model.

This model, while doing a satisfactory job at describing subject behavior, is not based on any known brain mechanisms. Furthermore, it makes no predictions beyond describing the behavioral observations in their experiment. Finally, the way they measure synchrony has nothing to do with the phase relationships between the two V-cell responses over time and simply measures response overlap. An ideal synchrony metric would capture the phase relationships between the two outputs and would preferably be normalized to a restricted range such as [0, 1].

3.2. Hodgkin-Huxley (1952)

In 1952, Hodgkin and Huxley proposed a neural model based on the biophysics of neural ion currents and membrane potentials. This model is widely regarded as the most accurate description of neural firing to date and has successfully predicted behaviors beyond what Hodgkin and Huxley originally observed at the time of their research. In my research, I adopt a neural architecture consisting of four networked Hodgkin and Huxley neurons as shown in Figure 20. In this architecture two excitatory neurons (E_1 and E_2) receive stimulus-based input (e.g. from the LGN). These two neurons each have excitatory connections with inhibitory neurons (I_1 and I_2) which inhibit the excitatory neurons. Finally, the two excitatory neurons make connections with each other that may be excitatory, inhibitory or they may not be connected at all depending on the spatial configuration of the receptive fields in question.

Each neuron is described by four basic equations. The four equations for one neuron are:

$$\begin{aligned}\frac{dV}{dt} =& \frac{1}{\tau_V}\big(-(17.81 + 47.58V + 33.8V^2)(V - 0.48) \\ & - 26R(V + 0.95) - 1.93C(1 - 0.5H)(V - 1.4) - 3.25H(V + 0.95) \\ & - EE \cdot G_{EE}(V + 0.92) \\ & - IE \cdot G_{IE}(V + 0.92) \\ & - EI \cdot G_{EI}V + Input\big)\end{aligned} \tag{8}$$

$$\frac{dR}{dt} = \frac{1}{\tau_R}\big(-R + 1.29V + 0.79 + 3.3(V + 0.38)^2\big) \tag{9}$$

$$\frac{dC}{dt} = \frac{1}{\tau_C}\big(-C + 6.65(V + 0.86)(V + 0.84)\big) \tag{10}$$

$$\frac{dH}{dt} = \frac{1}{\tau_H}(-H + 3C) \tag{11}$$

The main equation governing the neuron's voltage over time is the dV/dt equa-

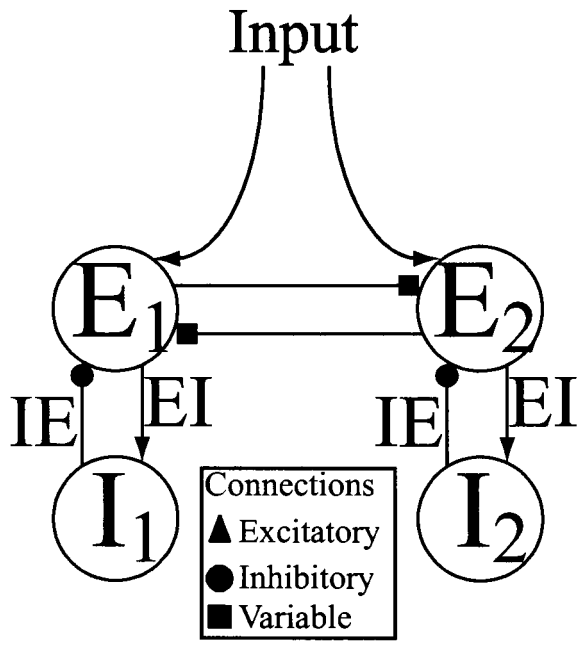

Figure 20. Schematic demonstrating networking between neurons. Arrows indicate excitatory connections, filled circles indicate inhibitory connections and squares indicate connections that may be either excitatory or inhibitory depending on the two neurons' receptive field configuration. E_1 and E_2 are excitatory neurons and I_1 and I_2 are inhibitory.

tion. This equation saturates with increasing voltage due to the negative coefficients on V appearing on the right hand side of the differential (meaning that V's rate of change decreases with increasing V), producing spikes with a rapid fall-off in voltage. The dV/dt equation is modulated by the three remaining equations. The dR/dt equation regulates recovery from spiking and takes on increasing values with increasing voltage, but in turn helps to decrease the values in the dV/dt equation with increasing voltage. The dC/dt equation represents the Ca^{2+} conductance across the neural membrane and the current controlled by C triggers action potential bursts. The variable C also increases the neuron's internal Ca^{2+} concentration, represented by the variable H, by providing input to the dH/dt equation. The variable H represents Ca^{2+} -modulated K^+ channel conductance, which functions on a much slower time scale than C.

Different cells are networked together through Rall's alpha function (Rall, 1967):

$$\frac{dF}{dt} = \frac{1}{\tau_{syn}}\big(-F + H_{step}(V_{pre} - \Omega_{Syn})\big) \tag{12}$$

$$\frac{dG}{dt} = \frac{1}{\tau_{syn}}(-G + F) \tag{13}$$

where

$$H_{step}(x) = \begin{cases} 1 & \text{if } x > 0 \\ 0 & \text{if } x \leq 0 \end{cases} \tag{14}$$

and V_{pre} is the voltage at the presynaptic neuron and Ω_{Syn} is the neuron's firing threshold.

Excitatory neurons (E_1 and E_2) are parameterized such that EI = 0 in the $\frac{dV}{dt}$ equation (Equation 8) and the connection from E_2 to E_1 passes through Rall's alpha function as:

$$\frac{dF_{E_2 \to E_1}}{dt} = \frac{1}{\tau_{syn}}\big(-F_{E_2 \to E_1} + H_{step}(V_{E_2} - \Omega_{Syn})\big)$$

$$\frac{dG_{EE}}{dt} = \frac{1}{\tau_{syn}}(-G_{EE} + F_{E_2 \to E_1})$$

and similarly the connection from E_1 to E_2 passes through Rall's alpha function as:

$$\frac{dF_{E_1 \to E_2}}{dt} = \frac{1}{\tau_{syn}}\big(-F_{E_1 \to E_2} + H_{step}(V_{E_1} - \Omega_{Syn})\big).$$

$$\frac{dG_{EE}}{dt} = \frac{1}{\tau_{syn}}(-G_{EE} + F_{E_1 \to E_2})$$

Similarly the connection from an inhibitory neuron to its corresponding excitatory

neuron passes through Rall's alpha as:

$$\frac{dF_{I\to E}}{dt} = \frac{1}{\tau_{syn}}\left(-F_{I\to E} + H_{step}(V_I - \Omega_{Syn})\right)$$
$$\frac{dG_{IE}}{dt} = \frac{1}{\tau_{syn}}(-G_{IE} + F_{I\to E})$$

Inhibitory neurons are parameterized such that IE = 0, EE = 0 and EI = 2 in Equation 8 and the connection from excitatory to inhibitory neurons passes through Rall's alpha function as:

$$\frac{dF_{E\to I}}{dt} = \frac{1}{\tau_{syn}}\left(-F_{E\to I} + H_{step}(V_E - \Omega_{Syn})\right)$$
$$\frac{dG_{EI}}{dt} = \frac{1}{\tau_{syn}}(-G_{EI} + F_{E\to I}).$$

For eliciting synchrony, no coupling or asynchrony I used the excitatory-excitatory (EE) and inhibitory-excitatory (IE) connection weights given in Table 1 below.

Table 1. Excitatory-excitatory and inhibitory-excitatory connection weights.

Neural Behaviour	EE	IE
Synchrony	-33	-30
No Coupling	0	0
Asynchrony	27	30

The constants I used (based on Hodgkin and Huxley's original work) are given in Table 2.

Figure 22 illustrates this model's behavior under three different E_1-E_2 connection parameterizations (EE) for inputs that are temporally 45° out of phase. The way the model handles the input depends on the receptive field configuration of the neurons receiving the inputs (Figure 21). When the receptive fields are perpendicular (Figure 21 top), EE is set to +27 and the model exhibits asynchronous coupling causing the spike trains line up in antiphase and producing outputs that are less

Table 2. Constants used in my modeling.

Variable Symbol	Value	Description
τ_V	0.97	Neural time constant (msec)
τ_R	5.6	Recovery time constant
τ_C	30	Time constant for Ca^{++} entry
τ_H	100	Time constant for inhibitory after-hyperpolarizing potential
τ_{Syn}	40	Inhibitory post-synaptic potential time constant
Ω_{Syn}	-0.2	Threshold for IPSP conductance change
EI	2	Excitatory-inhibitory weight
EE	variable	Excitatory-excitatory coupling coefficient
IE	30	Inhibitory-excitatory weight

synchronous than the inputs (Figure 22D). When the receptive fields are co-circular or collinear (Figure 21 bottom), EE is set to -33 and the model exhibits synchronous coupling yielding spike trains that line up with each other and produce outputs that are more synchronous than the inputs (Figure 22C). When the receptive fields are intermediate between perpendicular and collinear, EE is set to zero and the model exhibits no coupling and the spike trains phase lock with the input stimulus (Figure 22B).

This model is capable of producing behavior that is uncoupled, synchronously coupled or asynchronously coupled while retaining biophysical plausibility and, as shall be seen shortly, predicts the gamma range power that has been observed in electrophysiological studies of perceptual grouping.

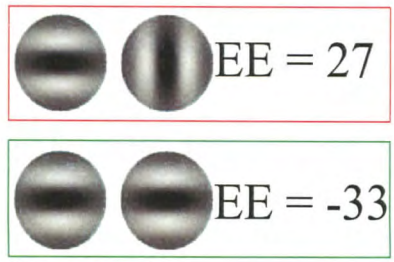

Figure 21. EE values as a function of receptive field configuration. Top: for orthogonal receptive fields EE takes on a value of 27 thereby desynchronizing the inputs. Bottom: for collinear receptive fields EE takes on a value of -33 thereby synchronizing the inputs.

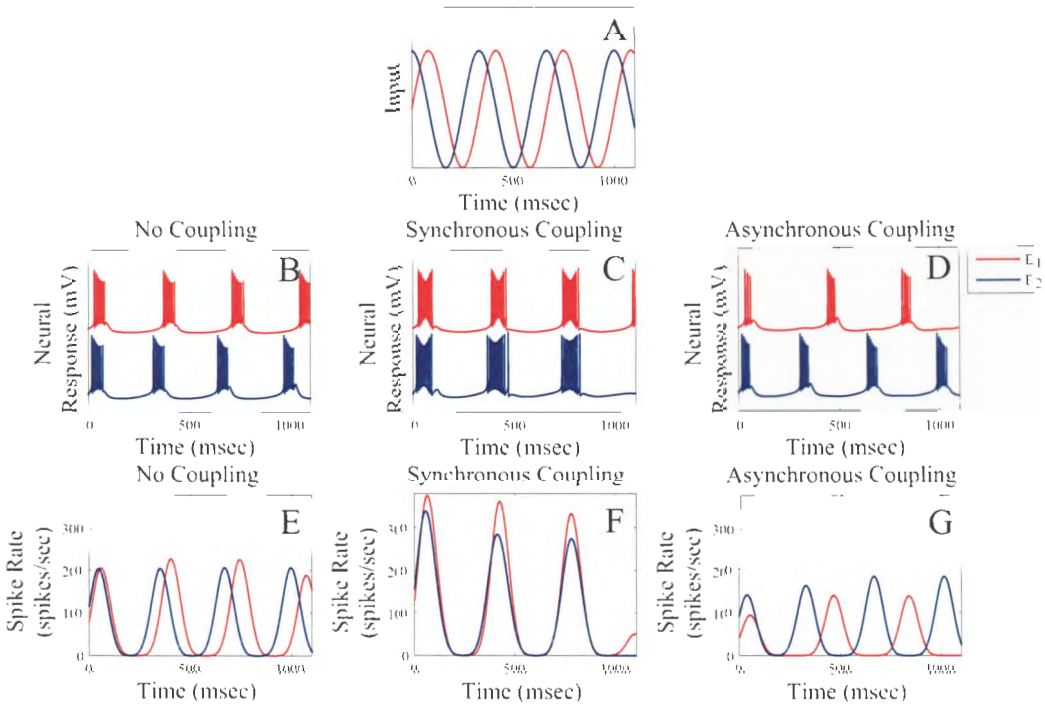

Figure 22. Model inputs are shown on the top in A. Model outputs are shown in the bottom for B: no coupling, C: synchronous coupling, and D: asynchronous coupling. Note that for the synchronously coupled neurons the outputs are more synchronous than the inputs, while for the asynchronously coupled neurons the outputs are less synchronous than the inputs. Plots E, F and G show spike rates for B, C and D respectively and are more similar to Cheadle et al.'s model outputs shown in Figure 18 than are the raw spike plots, suggesting Cheadle et al.'s model may be best suited as a description of spike rates rather than membrane voltages. Note in these plots that the neural spike rates go well into and even beyond the gamma range during bursting.

CHAPTER 4. MEASURING SYNCHRONY

There are many ways to measure synchrony. While each has its virtues, I develop here a measure that is best suited to the needs of this research.

Synchrony (Ψ) for two sinusoids with equal amplitudes and frequencies, like those shown in Figure 18A, may be intuitively defined as the phase difference between the two sinusoids:

$$\Psi = \phi_1 - \phi_2 \tag{15}$$

where ϕ_i denotes the phase of sinusoid i. This metric lies on the range $[-\pi, \pi]$ (given that care is taken to wrap differences greater than π or less than $-\pi$ as in Figure 23) and takes on a value of 0 radians when the two sinusoids are perfectly synchronous and takes on a value of either $-\pi$ or π radians when the two sinusoids are perfectly asynchronous. In order to restrict this measure to a more useful range and to assign a single number to asynchronous cases the synchrony measure may be modified as follows:

$$\Psi = 1 - \frac{|\phi_1 - \phi_2|}{\pi} \tag{16}$$

This dimensionless metric now lies on the range [0, 1] and takes on a value of 0 when the two sinusoids are perfectly asynchronous and a value of 1 when the two sinusoids are perfectly synchronous and is similar to the wavelet-based synchronization metric of Hramov and Koronovskii (2004).

Real world signals are rarely pure sinusoids with equal amplitudes, so a generally useful synchrony metric requires a bit more complexity. If the signal's true amplitudes are allowed to differ (let's call them A_1 and A_2) then this constitutes another form of asynchrony. An amplitude-difference-based synchrony metric might reasonably take the form:

$$\Psi = |A_1 - A_2| \tag{17}$$

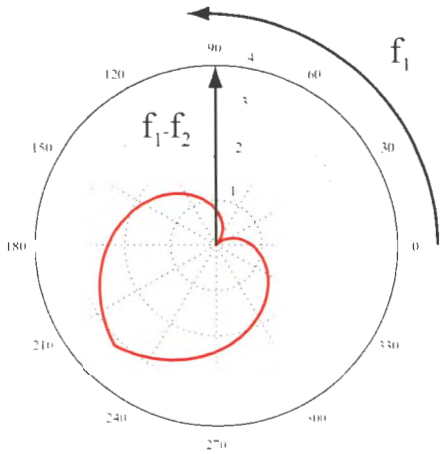

Figure 23. Difference between phases: $\phi_1 - \phi_2$. Here ϕ_2 is held fixed at 45° while ϕ_1 is rotated around the clock from 0° to 360°. Note the symmetrical form of the difference function for both clockwise and counterclockwise deviations from 45°.

This metric lies on the range $[0.\ \infty)$ and takes on a value of 0 when the two sinusoids have the same amplitudes at the same time and a value of ∞ when the two sinusoids have infinitely different amplitudes. Unlike the phase difference between two sinusoids, the amplitude difference between two sinusoids is unbounded in the positive direction. In order to restrict this measure to a more useful range the exponential function may be applied:

$$\Psi = \exp\left(-|A_1 - A_2|\right) \tag{18}$$

This metric now lies on the range $[0.\ 1]$ and takes on a value of 0 when the two sinusoids are infinitely asynchronous and a value of 1 when the two sinusoids are perfectly synchronous.

A synchrony measure that combines both phase and amplitude information takes the mean of these two synchrony measures:

$$\Psi = \frac{1 - \frac{|\phi_1 - \phi_2|}{\pi} + \exp\left(-|A_1 - A_2|\right)}{2} \tag{19}$$

This metric again lies on the range $[0.\ 1]$ and takes on a value of 1 for perfectly synchronous signals and a value of 0 for infinitely asynchronous signals. Figure 24

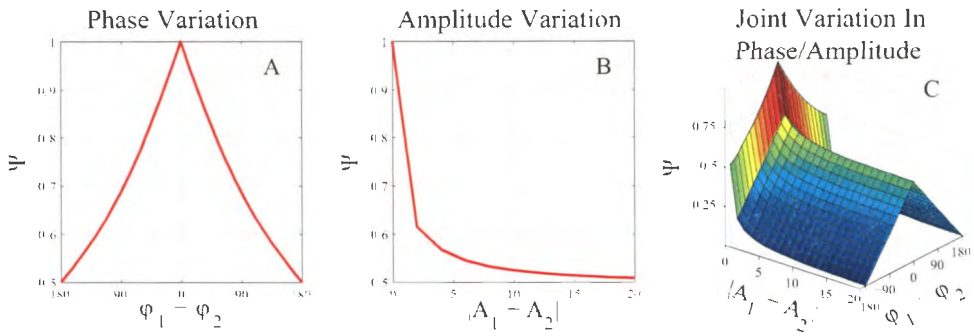

Figure 24. Synchrony measure Ψ as a function of A) signal phase difference, B) signal amplitude difference and C) joint phase and amplitude differences.

shows the result of applying this synchrony metric to sinusoidal signals with different phases (A), amplitudes (B) and jointly varying phases and amplitudes (C).

Real world signals rarely contain sinusoids of a single frequency. Fortunately, however, Fourier (1822) showed that all signals can be broken down into a sum of sinusoids with different frequencies. This fact allows synchrony to be computed within an arbitrary frequency band for an arbitrary signal. This is highly useful because some frequency bands have been postulated to be more important than others for cortical processing and perceptual grouping. In particular, several authors have found cortical synchrony in the gamma range (20 - 100 Hz) during perceptual grouping tasks both electrophysiologically and neurophysiologically (Engel et al., 1991a; Gray et al., 1989). Fourier's original work showed that a whole signal (from start to finish) could be reconstructed with a sum of sine and cosine waves of different frequencies, amplitudes and phases. Building on this work, Gabor (1946) further demonstrated that smaller, local pieces of a signal could be reconstructed based on a similar principle if the sine and cosine waves were enveloped by a Gaussian window. This led to what is currently known as a *wavelet transform*. Figure 25 gives an intuition of what a wavelet transform accomplishes. The top panel shows a pure sinusoid with a constant frequency (period = 200 milliseconds) oscillating through time. The bottom panel shows that signal's wavelet transform. Note that the peak amplitude occurs at the

signal's period (200 miliseconds, or 5 Hz) and that the phase changes as the signal oscillates through time.

For an arbitrary time-varying signal, $V(t)$, the signal's wavelet transform may be achieved by convolving the signal with a quadrature phase Gabor pair (the wavelets), where an individual Gabor is represented by $G(t)$ (Gabor, 1946).

A Gabor is essentially a sinusoid with a unique frequency that is enveloped by a Gaussian window. The equations for quadrature phase Gabor pairs are:

$$G_{\sin}(t;\omega,\sigma) = \sin(2\pi t\omega)\exp\left(-\left(\frac{t}{\sigma}\right)^2\right) \tag{20}$$

$$G_{\cos}(t;\omega,\sigma) = \cos(2\pi t\omega)\exp\left(-\left(\frac{t}{\sigma}\right)^2\right) \tag{21}$$

where t is time, ω is frequency and $\sigma = 1/\sqrt{\pi}$ is the envelope standard deviation. Examples of such Gabor functions are given in Figure 26.

In one dimension convolution is defined as:

$$[V * G](t) \equiv \int_{-\infty}^{\infty} V(\tau)G(t-\tau)d\tau \tag{22}$$

Here $*$ denotes the convolution operation, which is being performed on the functions $V(t)$ and $G(t)$ that are both functions of time (t). If both V and G lie on the range [-1 1] then convolution is essentially a template matching operation where the convolution result will take a large value at locations where the function V matches the function G and will take a lower value the worse the match between V and G.

For the purposes of this study, the signals of interest are neural membrane potentials given by Equation 8. Convolving the neurons' output voltages with quadrature phase Gabor pairs at a given frequency allows for an estimate of the amplitude and phase of those output voltages at the given frequency (ω) and at each time point (for

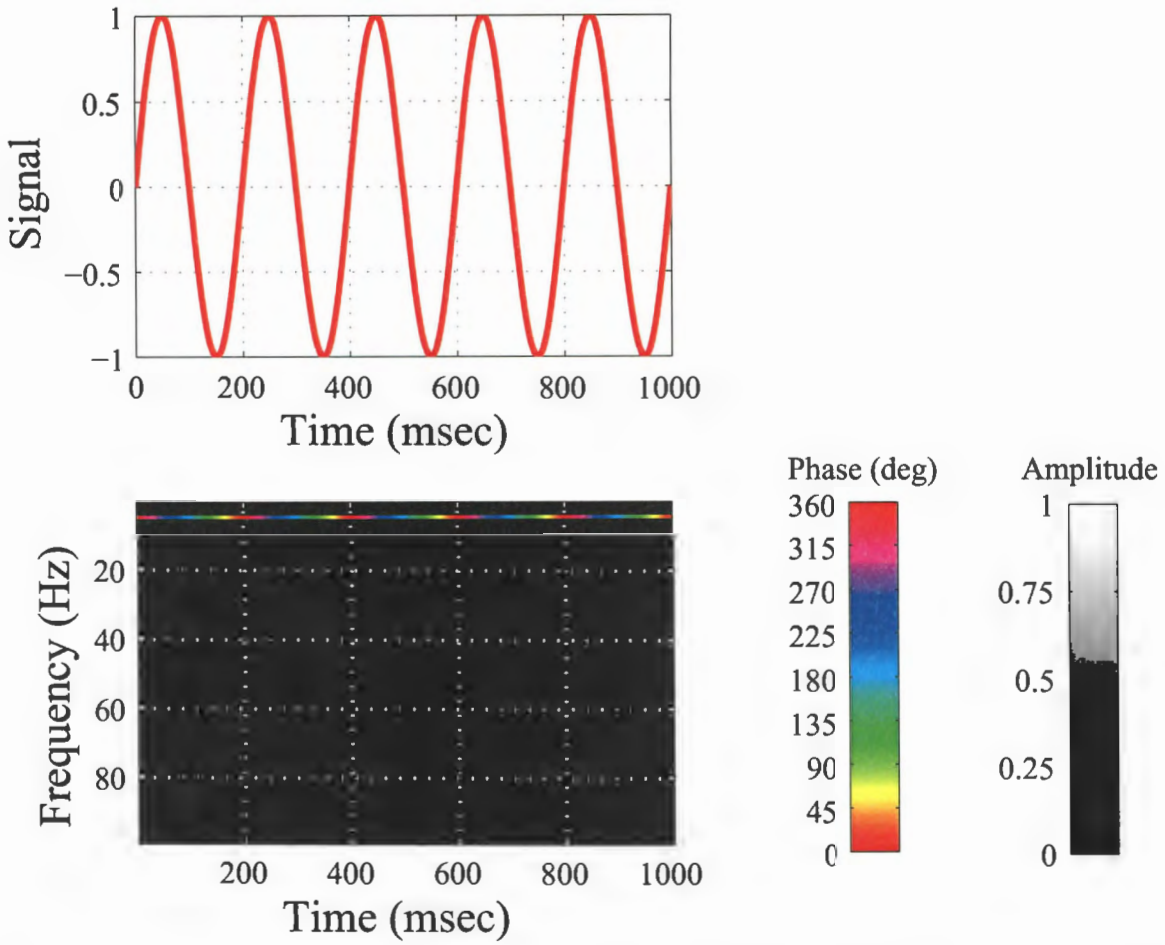

Figure 25. Top: Input signal to be wavelet transformed. Abscissa plots time against the signal on the ordinate. Bottom: Wavelet transform. Abscissa plots time against period on the ordinate (or 1/frequency). Different colors denote different phases and different lightnesses denote different amplitudes.

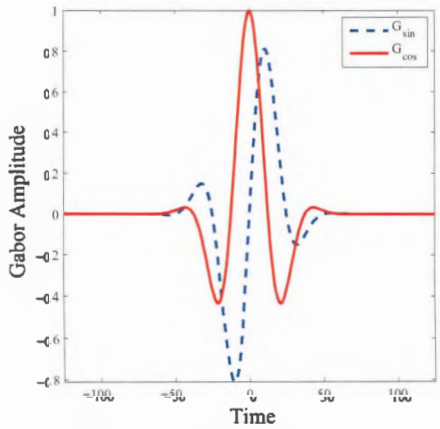

Figure 26. Two Gabors in quadrature phase.

an example see Figure 27). The amplitude at a given frequency is given by:

$$A(\omega) = \sqrt{(V * G_{sin}(\omega))^2 + (V * G_{cos}(\omega))^2} \tag{23}$$

and the phase by

$$\phi(\omega) = \arctan \frac{(V * G_{sin}(\omega))}{(V * G_{cos}(\omega))} \tag{24}$$

where *arctan* is the arctangent function.

Performing this operation for all frequencies allows one to estimate a signal's instantaneous phase and amplitude for each of those frequencies at each time point as shown in Figure 25.

Having obtained phase-amplitude spectra for each of the output signals of the kind shown in Figure 22 one can measure the phase/amplitude similarity of the two signals within any desired frequency band by applying Equation 19.

In some cases it is desirable to have a synchrony metric that integrates information across frequencies. One might intuitively define such a metric as a simple average of the synchronies obtained within each frequency band:

$$\Psi = \sum_{\omega \in \Omega} \frac{\Psi(\omega)}{N_\Omega} \tag{25}$$

where $\Psi(\omega)$ denotes the synchrony within the frequency band ω, Ω is the set of all frequencies present in the signal and N_Ω is the size of that set. One problem with this metric, however, is that it is subject to noise introduced by comparing the phases at frequencies with low amplitudes. When the amplitude is very close to zero phase measurements become highly uncertain and corrupt the synchrony measurements. Taking a weighted average alleviates this problem. Here, higher weights are assigned to frequencies with higher amplitudes and lower weights are assigned to frequencies

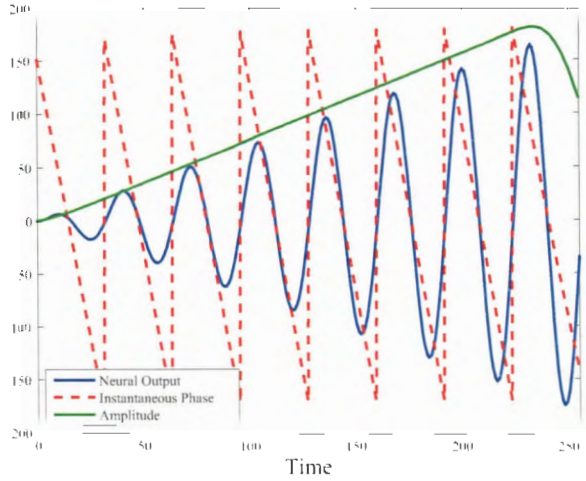

Figure 27. Phase/Amplitude decomposition for an arbitrary neural output. Abscissa plots time while ordinate plots the original signal's magnitude, the signal's phase and the signal's amplitude for the blue, red and green lines respectively. Here a sinusoidal signal (blue dot-dashed line) maintains a constant frequency but changes phase periodically and increases in amplitude monotonically. The red dashed lines show the instantaneous phase and the green solid line the instantaneous amplitude as computed by a wavelet transform.

with lower amplitudes. This converts Equation 25 to:

$$\Psi = \sum_{\omega \in \Omega} w_\omega \cdot \Psi(\omega) \tag{26}$$

where

$$w_\omega = \frac{A(\omega)}{\sum_{\omega \in \Omega} A(\omega)}. \tag{27}$$

Similarly, one may wish to integrate synchrony measures over time. This may be achieved by averaging Equation 26 over time:

$$\Psi = \sum_{t \in T} \sum_{\omega \in \Omega} w_\omega \cdot \frac{\Psi(\omega, t)}{N_T} \tag{28}$$

where T is the set of all discrete times being integrated over and N_T is the size of this set.

This measure of synchrony is superior to Cheadle et al.'s measure (Equation

7) for two main reasons. The first is that synchrony is defined directly in terms of the phase and amplitude relationships between sinusoidal waveforms. Nowhere in Cheadle et al.'s formulation do they explicitly measure the phases of any waveforms associated with their neural outputs. Equation 28, on the other hand, directly measures the phases of the neural outputs' sinusoidal components and compares them between neural outputs. The second reason is that sinusoidal waveforms with power at multiple frequency bands may add their component waves such that the signals appear to overlap, while the phases at any given frequency may be completely different. Cheadle et al.'s measure would regard this case as synchronous when in fact the phases within each frequency band would actually be misaligned. Equation 28 allows the phase relationships between neural outputs within each frequency band to be analyzed independently of all the other frequency bands, therefore providing a maximally pure measure of the phase relationships between neural outputs and the best estimate of neural synchrony. Furthermore, this formulation allows for analysis of synchrony within particular frequency bands (e.g. the gamma band) that may be of theoretical interest, where Cheadle et al.'s measure does not.

A plot of the wavelet transform for a single neuron under the Hodgkin and Huxley (1952) model is shown in Figure 28. The subplot shown in Figure 28A reproduces one of the spike trains from Figure 22B. The subplot shown in Figure 28B shows this signal's wavelet transform. Note that the signal demonstrates power extending into the gamma range (20-100Hz) (see also Figure 22) during neural bursting.

A plot of the wavelet transform for a single model unit under the Cheadle et al. (2008) model is shown in Figure 29. The subplot shown in Figure 29A is the output of the Cheadle et al. (2008) model. The subplot shown in Figure 29B shows this signal's wavelet transform. Note that the signal does not demonstrate power extending into the gamma range, but instead simply has power at the input frequency of 5 Hz.

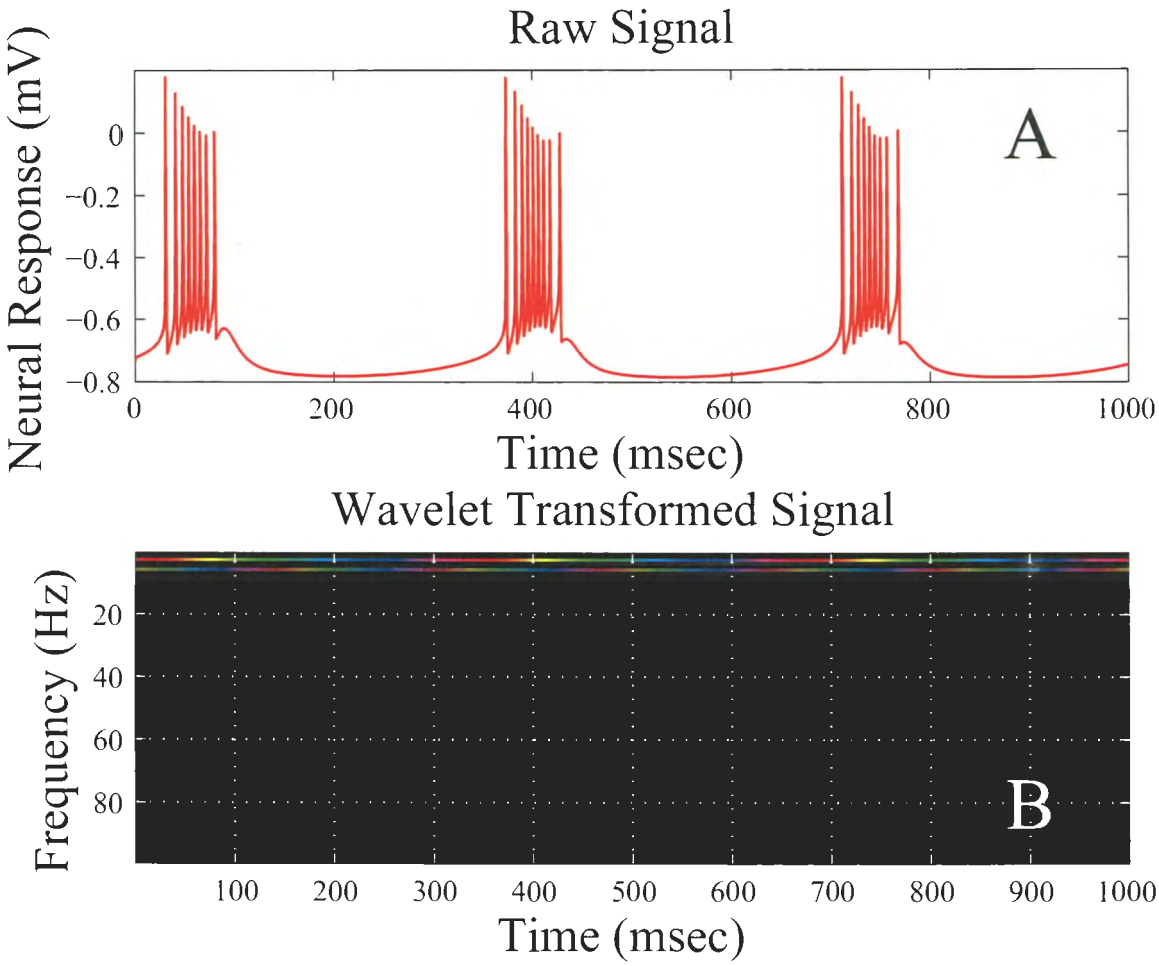

Figure 28. Demonstration of the wavelet transform on a Hodgkin and Huxley type neuron. A) the raw signal. B) The signal's wavelet transform. Color bars same as in Figure 25. Note that although most of the power in the wavelet transform is concentrated around the stimulus frequency, faint bars of power can be detected between 80 and 100 Hz (i.e. the gamma range).

These results indicate that the Hodgkin and Huxley (1952) based model is superior to the Cheadle et al. (2008) model, not only in accurately reproducing real neural spike trains, but also in eliciting gamma range activity even when the inputs to the model do not contain gamma frequency components (due to the rapid spikes within the bursts).

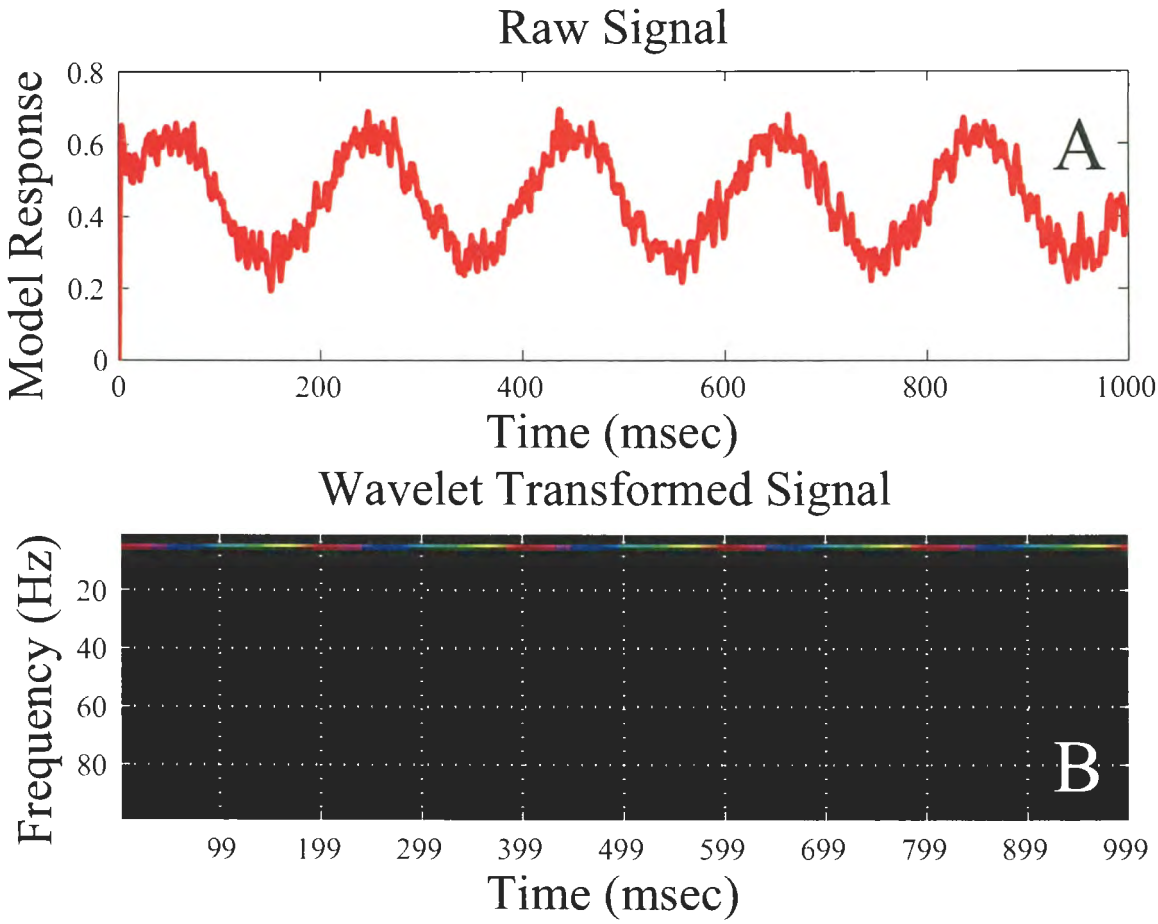

Figure 29. Demonstration of the wavelet transform on a Cheadle et al. (2008) type neuron. A) the raw signal. B) The signal's wavelet transform. Note the signal's power does not extend into the gamma range during spike bursts. Color bars same as in Figure 25.

CHAPTER 5. THE CURRENT STUDY

To summarize the key points so far, the prior literature suggests that neural synchrony may be implicated in perceptual grouping processes. Neurophysiological studies show that neurons whose receptive fields lie in line with an association field tend to synchronize. Computational modeling studies suggest that while primitive stimulus attributes, such as contrast, may be signalled via a rate code, more complex object membership relationships may be encoded via a synchrony code, interleaving synchronous bursts from cells responding to separate objects (i.e. temporal multiplexing). Behavioral studies reveal that synchrony sensitivity over different stimulus configurations is consistent with models where synchrony is imposed on stimulus elements projecting from a common object. There is a gap in the literature, however, because in order for temporal multiplexing to be effective the nervous system needs a mechanism by which to desynchronize signals projecting from separate objects. My neural modeling section provides a mechanism for how this may be achieved at the neural level. The current experiments will seek to provide behavioral evidence showing that human behavioral discriminations are consistent with a model that imposes asynchrony on representations of stimulus elements projecting from separate objects. Experiment 1 will test the hypothesis that humans perceive elements on separate objects to be less synchronous than elements on a common object and Experiment 2 will test the hypothesis that human sensitivity to stimulus synchrony/asynchrony falls in line with the predictions of a model that desynchronizes representations of elements projecting from separate objects.

CHAPTER 6. EXPERIMENT 1

6.1. Participants

Participants included two experienced psychophysical observers (one female) whose vision was either normal or corrected to normal and whose ages were 18 and 31. Participants gave informed written consent, and the study complied with the NIH standards of Human Participant Protection and was approved by North Dakota State University's IRB (protocol number SM06154). One participant was naïve to the study's purpose and the other was an author.

6.2. Apparatus

Stimuli were displayed on a 22 inch (56 cm) gamma-corrected Iiyama HM204DT Vision Master 514 CRT monitor (800 $\times$ 600 resolution, refresh rate 200 Hz) connected to a Macintosh Dual 2.7 GHz PowerPC G5 workstation with an ATI Radion X800 XT Mac Edition video card. At a viewing distance of 2 m the display monitor subtended 8.5 $\times$ 11.3 degrees of visual angle. Participants viewed the stimuli binocularly and their head position was stabilized using a chin rest. CRT luminance increments were linearized by a look-up-table (using a least-squares fit of a gamma function to the monitor's voltage-to-luminance transfer function) to give 10 bit intensity resolution. A Minolta LS-110 handheld photometer was used to calibrate the display screen. Responses were collected using a Logitech RumblePad 2 gamepad. Experiments were scripted in Matlab 7.2® using custom software and extensions from the PsychToolbox for OSX v. 10.4.11 (Brainard, 1997; Pelli, 1997).

6.3. Stimuli and Procedure

In this experiment I wish to test the hypothesis that image elements on separate objects are actively desynchronized relative to image elements on a common object. In

order to test this hypothesis I used the stimulus of Cheadle et al. (2008) that contains one object (Figure 17B), and I designed a new stimulus that contains two objects (Figure 17C). In each stimulus pattern two of the elements sinusoidally oscillated in their contrast (marked by red and blue circles in Figure 17) while the remaining elements remained fixed at 100% contrast. The stimulus duration was three seconds. Over the course of a contrast oscillation the Gabors' Michelson contrast ranged from zero to one. I designed the two-object pattern so that it exploited the Gestalt principles of proximity, similarity, symmetry, good continuation and closure (see Figure 12) to define object membership (Brunswik and Kamiya, 1953; Elder and Goldberg, 1998a,b; Elder and Zucker, 1996; Geisler et al., 2001; Koffka, 1935).

If the active desynchronization hypothesis is correct then participants should perceive the elements on a one-object pattern to be more synchronous and the elements on a two-objects pattern to be less synchronous than they are physically.

Stimuli were pre-computed for this experiment and were formed by placing Gabor patches on a lattice and varying their orientations (for a schematic see Figure 30). The full stimulus array subtended 3.7 $\times$ 3.7 degrees of visual angle and was composed of 9 $\times$ 9 evenly spaced Gabor patches with a center-to-center distance of 0.4 degrees of visual angle between neighboring Gabors. Each Gabor had an envelope standard deviation of 0.05 degrees of visual angle and a spatial frequency of 8.8 cycles per degree. On a single trial, subjects were presented with both a one-object pattern and a two-objects pattern simultaneously, with one pattern presented at the top of the display and the other pattern at the bottom (for a total height of 8.2 degrees).

In the one-object image proximity, similarity, symmetry and good continuation were leveraged to form a single, horizontal contour along the image's midline (all of the Gabors on the image's midline are horizontally oriented) while the remaining Gabors formed random background clutter (Figure 30 bottom). In the two-

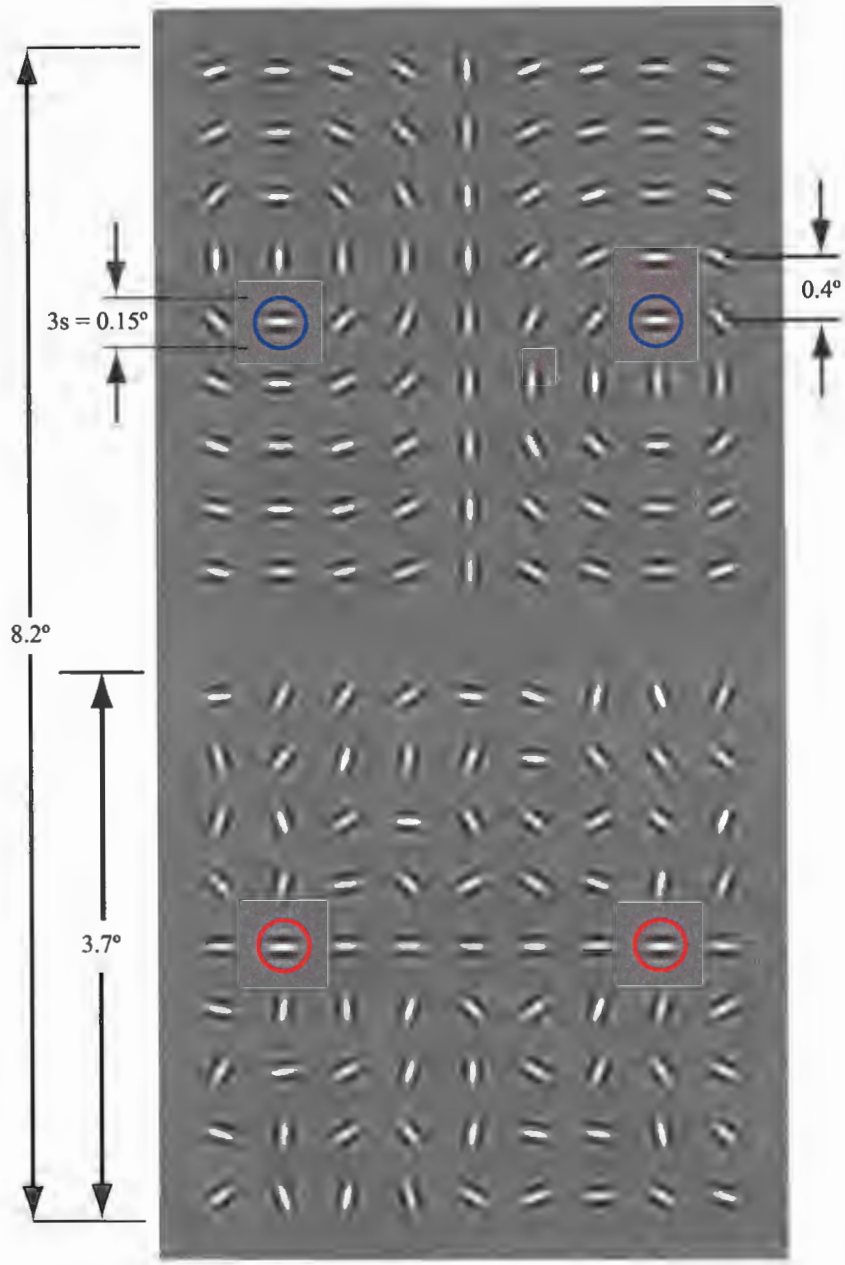

Figure 30. Stimulus schematic. The top pattern shows the two-objects pattern while the bottom pattern shows the one-object pattern. In both patterns, two of the Gabor patches in the same relative positions (marked by blue and red circles) were held fixed at a horizontal orientation. The Gabors in the two-objects pattern (circled in blue) always oscillated synchronously, while the Gabors in the one-object pattern (circled in red) varied in their synchrony level from trial to trial.

objects image proximity, similarity, symmetry, good continuation and closure were leveraged to compose two rings, where each ring was defined by proximal and co-

circular Gabor elements forming a closed structure (Figure 30 top). The number of objects in the stimulus constituted the first independent variable for this study. My empirical data bear out that participants perceive my two types of object stimuli differently. In each stimulus two of the Gabors on the horizontal meridian were always at the same orientation and position (marked by blue and red circles in Figure 30 but these marks were excluded in the stimulus presented to participants) and were separated by a center-to-center distance of 2.5 degrees of visual angle. These two Gabors sinusoidally oscillated in their contrast at a rate of 3 Hz (ranging from 0% contrast to 100% contrast) while the rest of the Gabors on the grid remained fixed at 100% contrast. The relative temporal phase of the two contrast-oscillating Gabors constituted the second independent variable in this study and was limited to the set $\phi \in [0°, 3°, 5°, 7°, 10°, 20°, 30°, 40°, 50°, 60°, 70°, 80°, 90°]$.

Stimulus Gabors were defined by the equation:

$$\begin{aligned} L(x,y) = \frac{1}{2\pi\sigma^2} \exp\left(-\frac{(x-\mu_x)^2 + (y-\mu_y)^2}{2\sigma^2}\right) \times \\ \cos\left(2\pi\lambda\big((x-\mu_x)\cos(\theta) + (y-\mu_y)\sin(\theta)\big) - \phi\right) - \\ \cos(\phi)\exp\left(\frac{-2\pi\sigma^2}{\lambda^2}\right) \end{aligned} \tag{29}$$

where L is the image luminance at a given position, x and y form a Cartesian coordinate system covering the image, μ_x is the x-coordinate of the Gabor's center, μ_y is the y-coordinate of the Gabor's center, σ controls the Gabor's spatial extent, λ controls the Gabor's period, θ controls the Gabor's orientation and ϕ controls the Gabor's phase. Gabors normally have a non-zero DC component for phase angles ϕ that are not 90°, however, the $\cos(\phi)\exp((-2\pi\sigma^2)/(\lambda^2))$ term in Equation 29 adjusts the Gabor's Fourier transform to have a zero DC component for all phase angles creating "balanced Gabors."

The two different object levels (one and two objects) were each generated in a particular fashion. For the one-object case (Figure 30 bottom), the orientations of all the Gabors lying on the horizontal meridian were clamped at horizontal while the remaining Gabors's orientations were sampled randomly and independently from a uniform distribution on the range $[0°, 360°]$. For the two-objects case (Figure 30 top), the Gabors were arranged in two concentric circles - one centered on the display's left half and the other on the display's right half, with the Gabors on the display's vertical midline clamped at a vertical orientation (i.e. $\theta = 0°$).

In the experiment participants completed a two-alternative-forced-choice task where they were asked to choose which of the two presented patterns (the top pattern or the bottom pattern) contained the *less* synchronously oscillating Gabors. Participants were instructed that they were to identify the pattern containing the less synchronous Gabor pair by making a button press (1 or 3 on the Game Pad indicating top or bottom respectively) and that the computer would record their selection. From trial to trial, the one-object pattern was randomly assigned to either the top or bottom of the display and the two-objects pattern was assigned to the remaining side. Across trials, the two-objects pattern always contained synchronously oscillating Gabors and the one-object pattern varied in the synchrony of its Gabors. Each run consisted of 240 trials, and trials were divided such that half of the presented stimuli had the same relative phase offsets (i.e. both top and bottom stimuli had a 0° phase offset). The remaining trials were evenly distributed among the remaining phase offsets for the one-object stimulus. This design ensures that chance performance is at 50% correct for the decision of which pattern was less synchronous. Over trials the computer stored the proportion of the time the participant identified the two-objects pattern as containing the more synchronously oscillating Gabors than the one-object pattern (i.e. proportion correct) at each phase offset.

With the given experimental design if subjects perform veridically then their performance should be at chance when the one-object pattern has a 0° phase offset (i.e. both one- and two-object patterns have identical phase offsets) and should be at 100% correct otherwise (Figure 31A). If subjects can not do the task then their performance should always be at chance (Figure 31B). Finally, if the experimental hypothesis is correct and subjects endogenously desynchronize the two-objects pattern relative to the one-object pattern then they should perceive the two-objects pattern to be less synchronous than the one-object pattern when they are equally matched and should reach the point of subjective equality at some non-zero phase offset, after which point their performance should eventually plateau (Figure 31C).

These three possibilities are easily distinguishable with a linear regression. If the veridical perception model is correct then a regression performed on the non-zero phase offsets should yield an intercept that is not significantly different from one and a slope that is not significantly different from zero. If the chance performance model is correct then a regression should yield an intercept that is not significantly

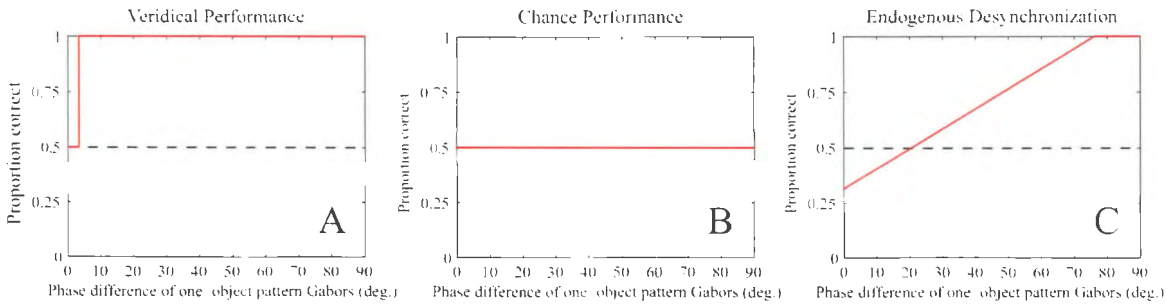

Figure 31. Possible experimental outcomes. (A) If subjects perform veridically then their performance should be at chance when the one-object pattern has a 0° phase offset (i.e. both one- and two-object patterns have identical phase offsets) and should be at 100% correct otherwise. (B) If subjects can not do the task at all then their performance should always be at chance. (C) If subjects endogenously desynchronize the two-objects pattern relative to the one-object pattern then they should perceive the two-objects pattern to be less synchronous than the one-object pattern when they are equally matched and should reach the point of subjective equality at some non-zero phase offset, after which point their performance should eventually plateau.

different from 0.5 and a slope that is not significantly different from zero. Finally, if the endogenous desynchronization model is correct then a regression should yield an intercept that is significantly lower than chance and a slope that is significantly greater than zero.

6.4. Results

Results from Experiment 1 are presented in Figure 32. Tables 3 and 4 summarize the regression statistics from Experiment 1. As can be seen by comparing Figure 32 with Figure 31, it is evident that the data support the endogenous desynchronization model. This subjective intuition is validated by the regression statistics in tables 3 and 4 where, as predicted by the endogenous desynchronization model, all intercepts were found to be significantly lower than chance and all slopes were found to be significantly greater than zero ($p < 0.05$).

Table 3. Regression Intercept Statistics From Experiment 1

Subject	Intercept		
	Value	Different from 0.5?	Different from 1?
AC	0.26	$t(10) = -8.50$, $p = 6.91 \times 10^{-6}$	$t(10) = -26.27$, $p = 1.47 \times 10^{-10}$
LH	0.37	$t(10) = -3.75$, $p = 3.76 \times 10^{-3}$	$t(10) = -18.48$, $p = 4.64 \times 10^{-9}$
Combined	0.32	$t(22) = -7.15$, $p = 3.61 \times 10^{-18}$	$t(22) = -26.66$, $p = 3.05 \times 10^{-18}$

Table 4. Regression Slope Statistics From Experiment 1

Subject	Slope	
	Value	Different from 0?
AC	0.01	$t(10) = 13.78$, $p = 3.94 \times 10^{-8}$
LH	0.01	$t(10) = 10.48$, $p = 5.17 \times 10^{-7}$
Combined	0.01	$t(22) = 14.51$, $p = 4.82 \times 10^{-13}$

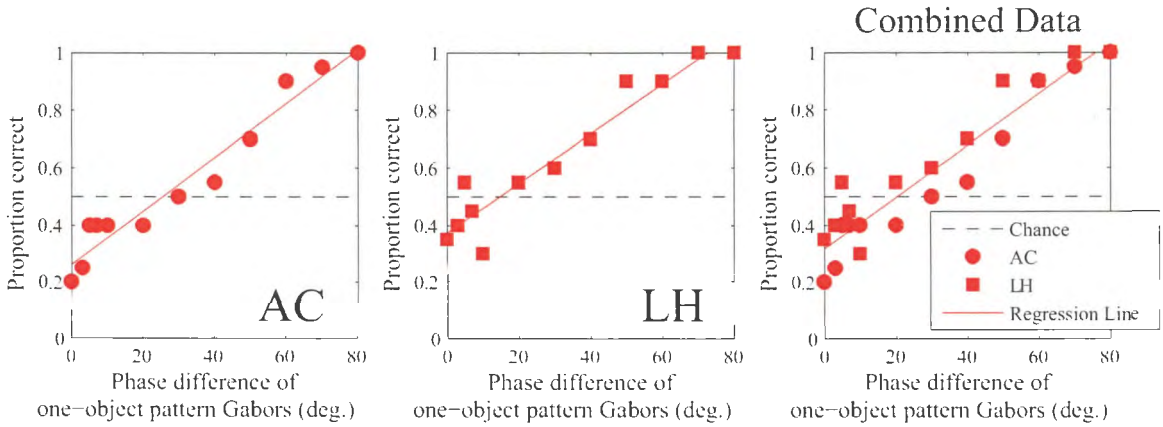

Figure 32. Experiment 1 results. Left panel - data for subject AC. Middle panel - data for subject LH. Right panel - combined data.

CHAPTER 7. EXPERIMENT 2

7.1. Participants

Participants included one female and three males whose vision was either normal or corrected to normal and whose ages ranged from 18 to 31. Participants gave informed written consent, and the study complied with the NIH standards of Human Participant Protection and was approved by North Dakota State University's IRB (protocol number SM06154). Three participants were naïve to the study's purpose and one was an author.

7.2. Apparatus

This experiment employed the same apparatus as Experiment 1, except that the viewing distance was changed to 150 cm due to an unavoidable change in testing rooms. At this new viewing distance the monitor subtended 11.3 × 15.0 degrees of visual angle.

7.3. Stimuli and Procedure

The results of Experiment 1 are subject to at least two possible criticisms. The first is that proportion correct is not an unbiased measure of sensitivity and, in effect, Experiment 1 essentially measured subjects' bias in their decisions about what kinds of patterns are perceived to be less synchronous. Although perceptual biases are interesting, it might also be interesting if sensitivity differences exist as well. The second criticism is that Experiment 1's two-objects pattern could possibly be interpreted by some as a pattern containing only one object. In order to strengthen my results and circumvent these two criticisms I designed Experiment 2 to measure subjects' *sensitivity* to synchrony and asynchrony as a function of whether the synchronous/asynchronous elements were parts of the same object of parts of different

objects. Furthermore, I designed new stimuli that yield more robust percepts of one and two objects.

For this experiment, stimuli were composed of Kanizsa figures (Kanizsa, 1976) where the inducers were arranged to yield percepts of either one or two objects. A schematic illustrating the stimuli employed in this experiment is shown in Figure 33. Each inducer's radius subtended 0.47 degrees of visual angle and the center-to-center distance between neighboring inducers was 1.88 degrees of visual angle. The center-to-center distance between the top inducers and the bottom inducers was 5.66 degrees of visual angle.

In each stimulus pattern (for both the top and bottom patterns in Figure 33) the four central inducers underwent 3 Hz sinusoidal contrast oscillations for 1.5 seconds while the remaining elements remain fixed at 100% contrast. Over the course of a contrast oscillation the Gabors' Michelson contrast ranged from zero to one with a polarity inversion such that the mean contrast was zero. The center-left inducers oscillated in perfect synchrony with each other, as did the center-right inducers, but the center-left and center-right inducers oscillated with a variable phase offset from each other.

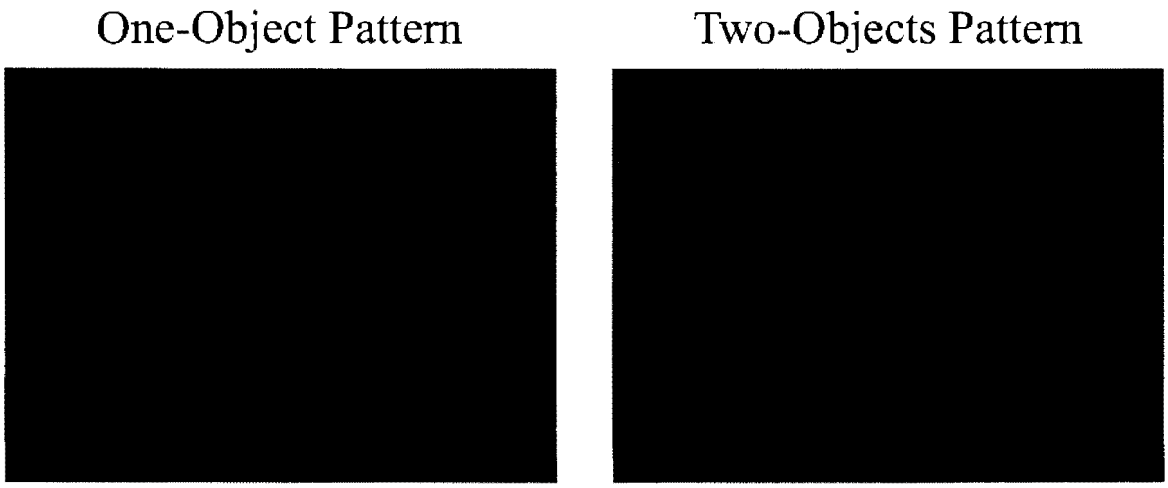

Figure 33. Schematic illustrations of the stimuli employed in Experiment 2. The left-hand image depicts the one-object stimulus, while the right-hand image depicts the two-objects image. Stimulus dimensions are given in degrees of visual angle.

For the top set of inducers, the phase offsets were limited to the set $\Delta\phi_{reference} \in [0°, 180°]$, while for the bottom set of inducers, the phase offsets were drawn from the set $\Delta\phi_{test} \in [0°, 15°, 30°, 45°, 60°, 75°, 90°, 105°, 120°, 135°, 150°, 165°, 180°]$. From trial to trial, subjects were required to perform a two-alternative forced-choice task where they indicated with a button press (1 or 3) whether the phase offset of the top inducer set was the same as the phase offset of the bottom inducer set. Trials were block-randomized such that 50% of the trials were the same and 50% were different. Furthermore, a block of phase offset comparisons was completed with only one object type (either Figure 33 left or right) before moving on to the next object type. Subjects were allowed to view each trial's stimulus multiple times before making their discrimination decisions.

This experimental design allows each subject's sensitivity to synchrony/asynchrony to be calculated via a measure called d'. According to signal detection theory, the results from the current method can be classified as shown in Table 5. Here, $p(Hit) + p(Miss) = 1$ and $p(FalseAlarm) + p(CorrectRejection) = 1$. Misses and correct rejections, therefor, provide redundant information as each can be calculated if one already knows the probabilities of hits and false alarms (F.A.). Using hits and

Table 5. Breakdown of possible real-world phase difference relationships and subject responses for Experiment 2.

		True phase difference relationship	
		Same	Different
What subject says	Same	Hit	False Alarm
	Different	Miss	Correct Rejection

false alarms, then one may calculate d' as illustrated in Figure 34 by taking

$$d' = Z(Hits) - Z(F.A.) \tag{30}$$

where $Z(\bullet)$ indicates that we are taking the z-score for the given quantity using the inverse cumulative normal function. This measure provides a sensitivity measure that is unaffected by the subject's decision bias. In terms of Figure 34, subjects are making classifications of "same" whenever they sample an internal signal that falls to the left of the vertical blue line. Regardless of where they decide to put this "criterion" line, however, the d' value will remain fixed as it is measuring the distance between the distributions and not where the criterion line (or bias) lies.

Some possible outcomes for this experiment are illustrated in Figure 35. If subjects are unable to perform the task, then their results should follow the patterns shown in Figure 35 A and B. Here, subjects sensitivity is zero over all test phase offsets. If subjects are able to perform the task, but they are unaffected by whether the contrast-oscillating inducers form part of the same object or parts of different objects then their results should follow the patterns shown in Figure 35 C and D. Here, sensitivity increases with increasing distance of the test phase offset from the reference phase offset, but there is no sensitivity difference between the one-object and two-objects curves (the red and blue curves). If subjects endogenously synchronize their internal representations of contrast-oscillating inducers forming part of a common object relative to inducers forming parts of different objects then their results should follow the patterns shown in Figure 35 E. Finally, if subjects endogenously desynchronize their internal representations of contrast-oscillating inducers forming parts of different objects relative to inducers forming part of a common object then their results should follow the patterns shown in Figure 35 F.

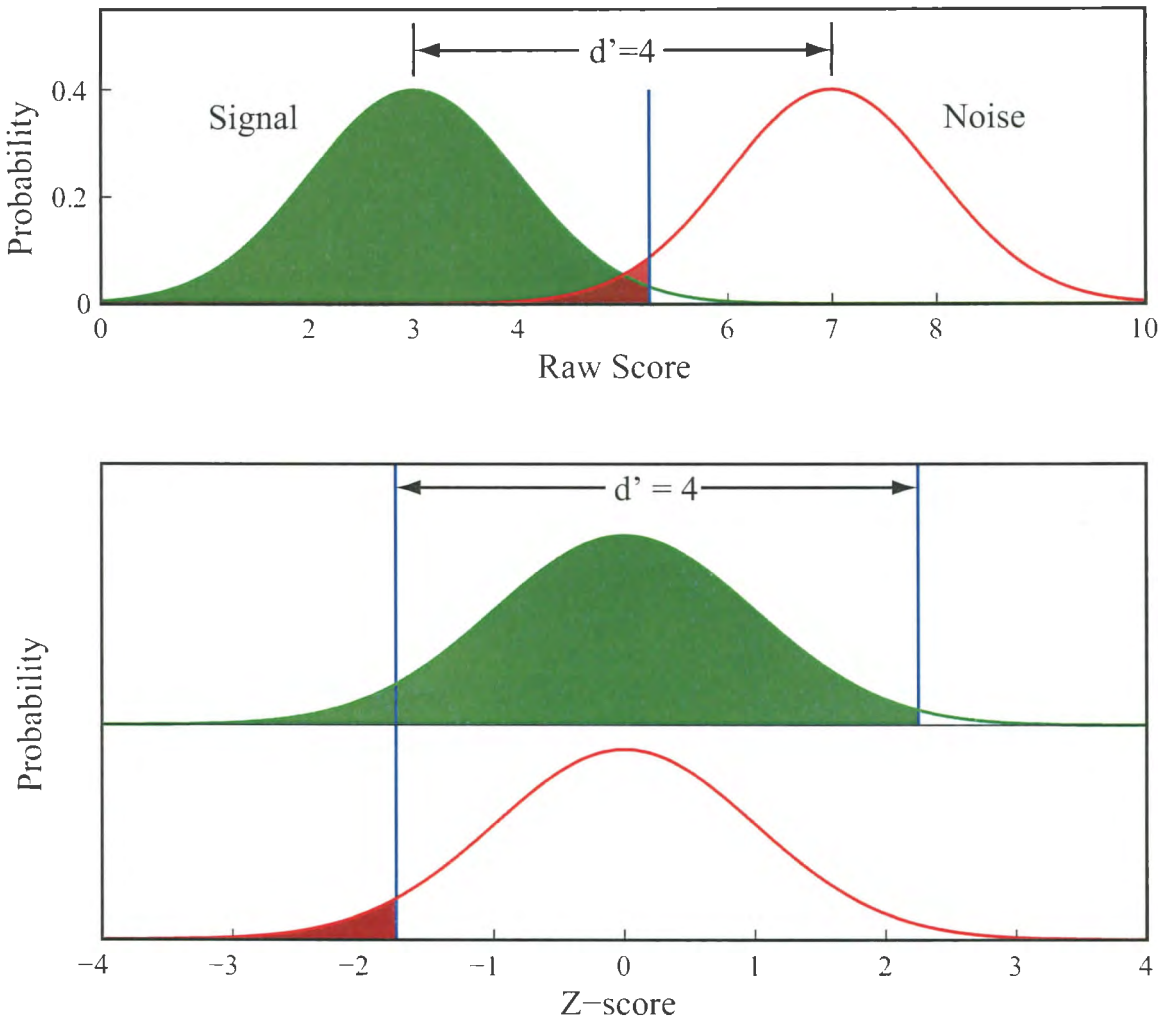

Figure 34. Sensitivity, as measured by d', is the distance between the signal and noise distributions in units of standard deviations. It may be calculated, as shown in the top panel, by measuring the number of standard deviations between the means of the raw distributions, or as shown in the bottom panel, by measuring the difference between z-scores for hits and false alarms on the z-normalized distributions, where the *hit* region is filled in green and the *false alarm* region is filled in red.

7.4. Results

Results from Experiment 2 are plotted in Figures 36 and 37. Figure 36 plots data for the 0° reference phase offset condition. Comparing this data with that presented in the left column of Figure 35, there are evidently some subtle differences between the curves for the one-object and two-objects data, but it is difficult to say whether the overall pattern most closely resembles Figure 35 C or E. Statistical

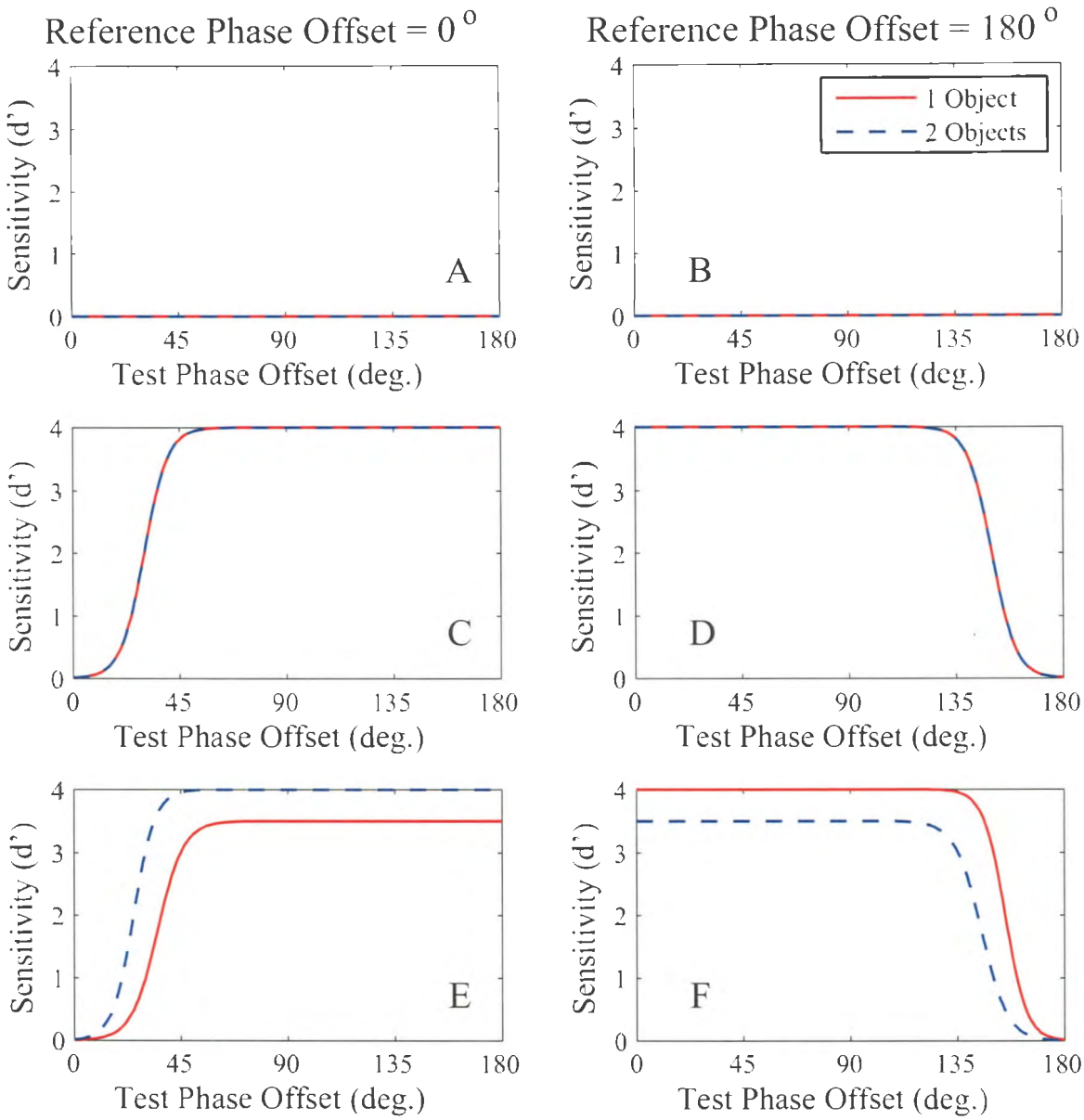

Figure 35. Three possible sets of outcomes for Experiment 2. In each plot, sensitivity is plotted against test phase offset for the one-object pattern (red lines) and the two-objects pattern (blue lines). The left plots show predictions for the case where the reference pattern is synchronous (i.e. $\Delta o_{reference} = 0°$) and the right plots show predictions for the case where the reference pattern is asynchronous (i.e. $\Delta o_{reference} = 180°$). A and B show predicted performance for the case where subjects are unable to perform the task. Here, sensitivity is always at zero for all test phase offsets. C and D show predicted performance for the case where subjects are able to perform the task, but where there is no difference in their ability to discriminate the test and reference phase offsets between the one- or the two-object patterns. E and F show predicted performance assuming an effect of the number of objects on sensitivity.

analysis using a two-factor repeated-measures ANOVA performed on the data shows a marginally significant difference between the one-object and two-objects pattern sensitivity measures over the test phase offsets ($F(1.3) = 8.95$, $p = 0.058$) and no significant interaction between number of objects and test phase offset ($F(11.33) = 1.97$, $p = 0.065 \rightarrow$ N.S.).

Figure 37 plots data for the 180° reference phase offset condition. Comparing this data with that presented in the right column of Figure 35, the data most closely resemble that presented in Figure 35 F, where subjects endogenously desynchronize the two-objects pattern relative to the one-object pattern. This intuition is also born out in the results of a two-factor repeated-measures ANOVA performed on the data showing a significant difference between the one-object and two-objects pattern sensitivity measures over the test phase offsets ($F(1.3) = 15.98$, $p = 0.028$) and no

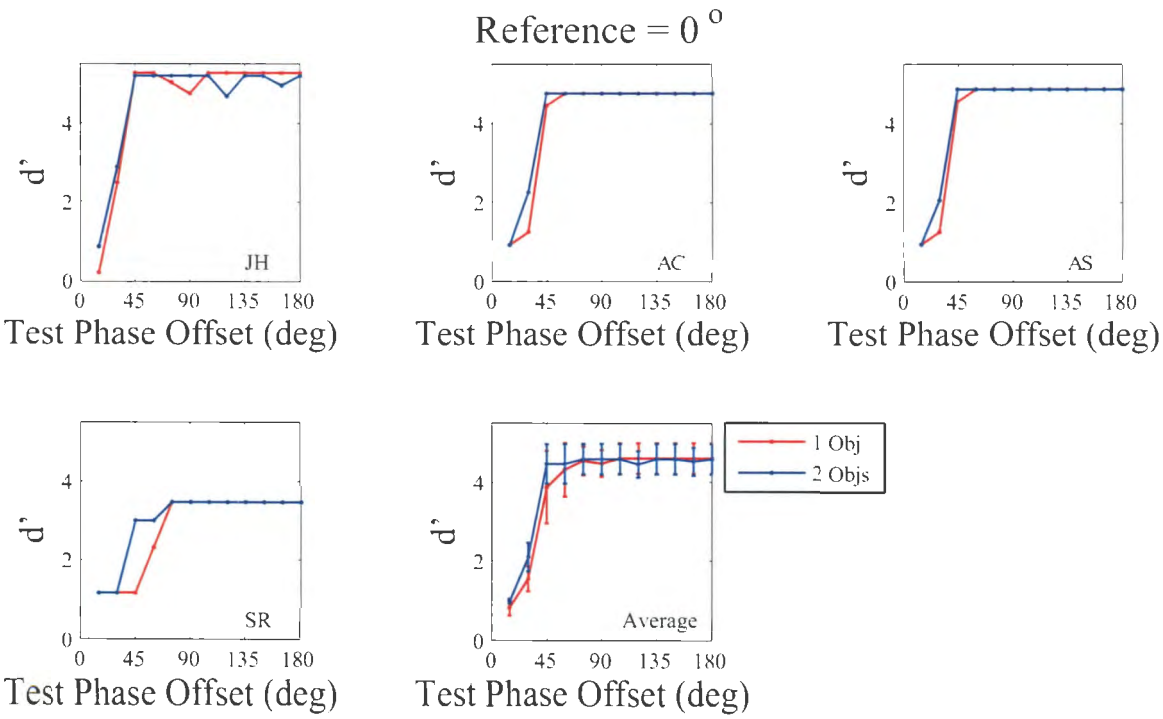

Figure 36. Results for Experiment 2 under the 0° reference phase condition (Compare to Figure 35 left column). The first four plots show individual subject data while the last plot shows the average over subjects with standard errors.

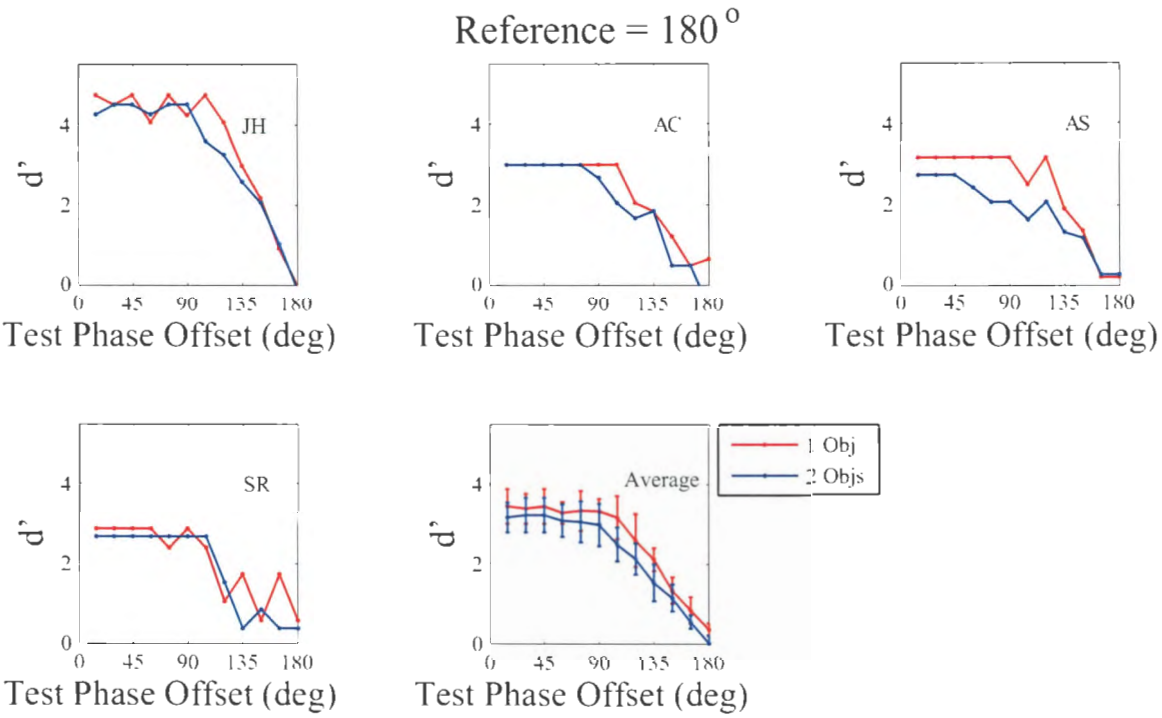

Figure 37. Results for Experiment 2 under the 180° reference phase condition (Compare to Figure 35 right column). The first four plots show individual subject data while the last plot shows the average over subjects with standard errors.

significant interaction between number of objects and test phase offset ($F(11.33) = 0.40$, $p = 0.944 \rightarrow$ N.S.).

For both the 0° and 180° references, there was a significant, but unsurprising effect of test phase offset on d' ($p < 0.05$), indicating that d', averaged over number of objects, was not constant across all phase offsets.

CHAPTER 8. DISCUSSION

The current experiment's results imply that subjects desynchronize their internal representations of elements lying on separate objects. To my knowledge, this is the first *behavioral* evidence supporting segmentation by asynchrony hypothesis first proposed by Yen et al. (1999).

Experiment 1's results show that when comparing flickering Gabors that form part of a common object with flickering Gabors that form parts of separate objects, subjects show a bias indicating that the elements on the separate objects are perceived as flickering less synchronously than are the elements on the common object. This bias is most clearly seen in Figure 32 when both the one-object and two-objects patterns contain perfectly synchronously flickering elements (i.e. test phase offset = 0°) and the intercept of the regression line deviates significantly below the 0.5 mark on the y-axis. This result implies that when synchrony is at ceiling levels and no further internal synchrony may be imposed on what is physically present in the stimulus, the subject internally represents the elements on the two-objects stimulus as being less synchronous than the elements on the one-object stimulus - implying that the subject is internally desynchronizing the elements on the two-objects stimulus. Beyond this point, when the test phase offsets are greater than zero degrees, it is reasonable to assume some mixture of internal desynchronization of the elements on the two-objects stimulus and internal synchronization of the elements on the one-object stimulus (Cheadle et al., 2008) accounts for the observed biases from veridical perception. The balance of this mixed bias doesn't reach the point of subjective equality (i.e. the point when proportion correct equals 0.5) until somewhere between 13° and 24° depending on the subject.

The results of Experiment 2 suggest that more than having a biased percept towards desynchronizing elements on a two-objects pattern relative to elements on

a one-object pattern, subjects are also less sensitive to test phase offsets for elements forming a two-objects pattern when the reference phase offset is perfectly asynchronous at 180°. Similarly, subjects are less sensitive to test phase offsets for elements forming a one-object pattern when the reference phase offset is perfectly synchronous at 0°. These results are exactly what one would expect if subjects were internally desynchronizing their representations of the elements on the two-objects pattern (see Figure 35 F) and synchronizing their representations of the elements on the one-object pattern (see Figure 35 E). To see why this is so, consider the function that relates the stimuli's physical phase difference to the subject's internal representation of that phase difference. Both physical and internal phase differences have minimum and maximum attainable values of 0° and 180° respectively, with 0° marking perfect synchrony and 180° marking perfect asynchrony. In the case of veridical perception, the function relating external to internal phase difference would be a straight line going from the point (0°, 0°) to (180°, 180°). Internal synchronization would manifest as deflections of this line towards an internal synchrony of 0° and internal desynchronization would manifest as deflections of this line towards an internal synchrony of 180°. In the case where the the stimuli's physical phase difference is 180° it is at the point where internal desynchronization can go no further. If subjects are internally desynchronizing the elements on the two-objects pattern, then their internal representation of those elements would remain at 180° for external phase differences that are less than 180°, thereby making the high end of phase differences indiscriminable to the subject and decreasing their sensitivity scores as measured by d'. Conversely, if subjects are internally synchronizing the elements on the one-object pattern, then their internal representation of those elements would remain at 0° for external phase difference that are more than 0°, thereby making the low end phase differences indiscriminable to the subject and decreasing their d' scores for phase

differences near 0°. These are exactly the patterns observed in the data and argue strongly for the binding by synchrony and segmentation by asynchrony hypotheses.

These results bear directly on object representation theories. Contrary to the views espoused by Shalden and Movshon (1999), the present results suggest that the brain does indeed use synchrony/asynchrony in a functional way - instead of representing the relative phases of contrast oscillating stimulus elements veridically, the visual system synchronizes or desynchronizes them depending on the static spatial context in which the elements are embedded. These findings lend support to the findings of many other researchers who have found a functional role for synchrony/asynchrony in the brain (Engel et al., 1991b,a,c; Gray et al., 1989; Fries et al., 2001; Roelfsema et al., 1997; Steinmetz et al., 2000; Singer, 2004; Kreiter and Singer, 1996; Fries et al., 2001; Roelfsema et al., 1997; Steinmetz et al., 2000; Engel et al., 1991c; Roelfsema et al., 1997; Herculano-Houzel et al., 1999; Munk et al., 1996; Kreiter and Singer, 1996; Cheadle et al., 2008). The implication of my research is that the brain is taking the original stimulus locked neural responses and modifying them to produce the observed behavior in a context-dependent way. Since the contrast oscillations in the one-object and two-objects stimuli were identical, the results suggest that the observed modulation in perceived synchrony is related to the different static backgrounds which were designed to elicit perceptual grouping and segmentation.

The brain is representing the exogenous signals presented in this experiment in a non-veridical way. I present a model for how this may be accomplished using standard biophysical modeling equations (Hodgkin and Huxley, 1952). The presented model (see Modeling section) demonstrates a simple and neurally plausible mechanism for implementing a synchronizing/desynchronizing circuit in the brain. The model's strengths are that it stems directly from biophysics, that it describes the current experimental findings and that it generalizes beyond these findings to explain why

electrophysiological experimenters observe gamma-range power when recording EEG signals from subjects performing perceptual grouping tasks.

Taken together, my behavioral results and my neural model bind together a parsimonious story for how the brain neurally represents information about local object membership - synch if they're the same and desynch if they're different.

Having covered the what and how of neural synchrony, I would now like to turn to the question of why the brain might want to impose illusory synchrony. The visual system could conceivably have been constructed to perceive the world veridically, but instead it imposes illusory synchrony in cases where elements lie on a common object and illusory asynchrony in cases where elements lie on separate objects. If the brain were merely using synchrony/asynchrony as labels for object membership then presumably it could have done so in a way that would not affect subjective percepts (one could imagine, for example, synchronizing/desynchronizing activity in the gamma range but leaving oscillations at the stimulus frequency veridical). What purpose does shifting the *perceived* synchrony level serve? The answer to this question might be more readily apprehended by examining the answer to a similar question. One could similarly ask, when examining Figure 16 (Kanizsa, 1976), why do subjects perceive edges that aren't actually there? The answer supported by the empirical evidence is that in the world we evolved in, edges that line up perfectly are usually connected, even if one can not detect the connection (Elder and Goldberg, 1998a,b; Geisler et al., 2001; Sigman et al., 2001; Elder and Goldberg, 2002), so seeing them as part of a connected whole will generally yield a veridical percept. Getting back to the question at hand, edges projecting from a common object will generally tend to appear and disappear at the same time, so seeing perfectly lined up edges as appearing and disappearing at the same time will generally facilitate veridical percepts. Furthermore, if the visual system does perform grouping by synchrony

and segregation by asynchrony then preparing a synchronous response to elements lying on a common object and preparing an asynchronous response to elements lying on separate objects will facilitate the process of making correct grouping and segmentation decisions in the future.

CHAPTER 9. CONCLUSIONS

In this paper I have demonstrated that normal observers endogenously synchronize or desynchronize their experiences of exogenously contrast oscillating stimulus elements depending on perceptual grouping cues present in the static patterns in which the oscillating elements are embedded. I have developed a biophysical neural model, based on the the work of Hodgkin and Huxley (1952) showing that this behavior may be reproduced at the neural level and have shown how this model is corroborated by separate electrophysiological and neurophysiological findings showing gamma frequency power in neural populations engaged in perceptual grouping tasks. Although neurons burst with an inter-burst frequency corresponding to the stimulus frequency, the pattern of firing within a burst is what elicits power in the gamma frequency range. Synchronized over a population of neurons this gamma frequency power is observable through large-scale brain recording techniques like EEG. The virtues of this model are that it is biophysically based, it successfully predicts both behavioral and electrophysiological results and it makes directly testable predictions on single cell neurophysiology and electrophysiology.

Importantly, I have provided new evidence suggesting that a mechanism used by the visual system is segregation by asynchrony. This finding complements prior results suggesting a role for grouping by synchrony and furthers our understanding of cortical mechanisms for scene segmentation.

BIBLIOGRAPHY

Adelson, E. H. and Bergen, J. R. (1985). Spatiotemporal energy models for the perception of motion. *Journal of the Optical Society of America A*, 2(2):284–299.

Albrecht, D. G., Geisler, W. S., Frazor, R. A., and Crane, A. M. (2002). Visual cortex neurons of monkeys and cats: Temporal dynamics of the contrast response function. *Journal of Neurophysiology*, 88:888–913.

Baumann, R., van der Zwan, R., and Peterhans, E. (1997). Figure-ground segregation at contours: a neural mechanism in the visual cortex of the alert monkey. *Eur. J. Neurosci.*, 9:1290–1303.

Blake, R. and Lee, S. H. (2005). The role of temporal structure in human vision. *Behavioral and Cognitive Neuroscience Reviews*, 4(1):21–42.

Blakeslee, B. and McCourt, M. E. (1999). A multiscale spatial filtering account of the white effect, simultaneous brightness contrast and grating induction. *Vision Research*, 39:4361–4377.

Brainard, D. H. (1997). The psychophysics toolbox. *Spatial Vision*, 10:443–446.

Brighina, F., Ricci, R., Piazza, A., Scalia, S., Gislia, G., and Fierro, B. (2003). Illusory contours and specific regions of human extrastriate cortex: evidence from rtms. *Eur. J. Neurosci.*, 17:2469–2474.

Brunswik, E. and Kamiya, J. (1953). Ecological cue-validity of proximity and of other gestalt factors. *American Journal of Psychology*, 66:20–32.

Burns, M. E. and Lamb, T. D. (2004). Visual transduction by rod and cone photoreceptors. In Chalupa, L. M. and Werner, J. S., editors, *The Visual Neurosciences*, chapter 16, pages 215–233. The MIT Press, Cambridge, Massachusetts.

Buzsaki, G. (1996). The hippocampo-neocortical dialogue. *Cerebral Cortex*, 6:81–92.

Buzsaki, G. and Chrobak, J. J. (1995). Temporal structure in spatially organized neuronal ensembles: a role for interneuronal networks. *Current Opinion in Neurobiology*, 5:504–510.

Campbell, F. W. and Robson, J. G. (1968). Application of fourier analysis to the visibility of gratings. *Journal of Physiology*, 197(3):551–566.

Carandini, M., Heeger, D. J., and Movshon, J. A. (1997). Linearity and Normalization in Simple Cells of the Macaque Primary Visual Cortex. *The Journal of Neuroscience*, 17(21):8621–8644.

Castelo-Branco, M., Goebel, R., Neuenschwander, S., and Singer, W. (2000). Neural synchrony correlates with surface segregation rules. *Nature*, 405:685–689.

Castelo-Branco, M., Neuenschwander, S., and Singer, W. (1999). Synchronization of visual responses between the cortex, lateral geniculate nucleus, and retina in the anesthetized cat. *The Journal of Neuroscience*, 18(16):6395–6410.

Cheadle, S., Bauer, F., Parton, A., Müller, H., Bonneh, Y. S., and Usher, M. (2008). Spatial structure affects temporal judgments: Evidence for a synchrony binding code. *Journal Of Vision*, 8(7):1–12.

Cope, D., Blakeslee, B., and McCourt, M. E. (2008). Structural theorems for simple cell receptive fields. *Journal of Vision*, 8(6):802.

Dacey, D. M. (1993). Morphology of a small-field bistratified ganglion cell type in the macaque and human retina. *Visual Neuroscience*, 10:1081–1098.

De Valois, R. L., Albrecht, D. G., and Thorell, L. G. (1982). Spatial frequency selectivity of cells in macaque visual cortex. *Vision Research*, 22:545–559.

Dresp, B. and Grossberg, S. (1997). Contour integration across polarities and spatial gaps: from local contrast filtering to global grouping. *Vision Research*, 37:913–924.

Elder, J. H. and Goldberg, R. M. (1998a). Inferential reliability of contour grouping cues in natural images. *Perception*, 27:11.

Elder, J. H. and Goldberg, R. M. (1998b). The statistics of natural image contours. *Proceedings of the IEEE CS Workshop on Perceptual Organization in Computer Vision.*

Elder, J. H. and Goldberg, R. M. (2002). Ecological statistics of gestalt laws for the perceptual organization of contours. *Journal of Vision*, 2:324–353.

Elder, J. H. and Zucker, S. (1996). Scale space localization, blur, and contour-based image coding. *Proc. IEEE Conference on Computer Vision and Pattern Recognition*, 20:27–34.

Elliott, M. A. and Müller, H. J. (1998). Synchronous information presented in 40-Hz flicker enhances visual feature binding. *Psychological Science*, 9:277283.

Engel, A. K., Fries, P., and Singer, W. (2001). Dynamic predictions: oscillations and synchrony in top-down processing. *Nature Reviews Neuroscience*, 2:704–716.

Engel, A. K., König, P., Kreiter, A. K., and Singer, W. (1991a). Interhemispheric synchronization of oscillatory neuronal responses in cat visual cortex. *Science*, 252:1177–1179.

Engel, A. K., König, P., and Singer, W. (1991b). Direct physiological evidence for scene segmentation by temporal coding. *The Proceedings Of The National Academy Of Sciences USA*, 88:9136–9140.

Engel, A. K., Kreiter, A. K., König, P., and Singer, W. (1991c). Synchronization of oscillatory neuronal responses between striate and extrastriate visual cortical areas of the cat. *The Proceedings Of The National Academy Of Sciences USA*, 88:6048–6052.

Fahle, M. (1993). Figure-ground discrimination from temporal information. *Proceedings of the Royal Society B: Biological Sciences*, 254:199203.

Farid, H. and Adelson, E. H. (2001). Synchrony does not promote grouping in temporally structured displays. *Nature Neuroscience*, 4:875–876.

Ffytche, D. and Zeki, S. (1996). Brain activity related to the perception of illusory contours. *Neuroimage*, 3:104–108.

Field, D. J., Hayes, A., and Hess, R. F. (1993). Contour integration by the human visual system: evidence for a local association field. *Vision Research*, 33(2):173–193.

Fourier, J. B. J. (1822). *La théorie analytique do la chaleur*. Firmin Didot, Paris, France.

Freiwald, W. A., Kreiter, A. K., and Singer, W. (1995). Stimulus dependent intercolumnar synchronization of single unit responses in cat area 17. *NeuroReport*, 6:2348–2352.

Fries, P., Reynolds, J. H., Rorie, A. E., and Desimone, R. (2001). Modulation of oscillatory neuronal synchronization by selective visual attention. *Science*, 291:1560–1563.

Fries, P., Roelfsema, P. R., Engel, A. K., König, P., and Singer, W. (1997). Synchronization of oscillatory responses in visual cortex correlates with perception in interocular rivalry. *Proceedings of the National Academy of Sciences of the USA*, 94:12699–12704.

Gabor, D. (1946). Theory of communication. *Journal of the Institution of Electrical Engineers*, 93:429–457.

Geisler, W. S., Perry, J. S., Super, B. J., and Gallogy, D. P. (2001). Edge co-occurrence in natural images predicts contour grouping performance. *Vision Research*, 41:711–724.

Goebel, R., Khorram-Sefat, D., Muckli, L., Hacker, H., and Singer, W. (1998). The constructive nature of vision: direct evidence from functional magnetic resonance imaging studies of apparent motion and motion imagery. *Eur. J. Neurosci.*, 10:1563–1573.

Gold, J. M., Bennett, P. J., and Sekuler, A. B. (1999). Signal but not noise changes with perceptual learning. *Nature*, 402:176–178.

Gold, J. M., Murray, R. F., Bennett, P. J., and Sekuler, A. B. (2000). Deriving behavioural receptive fields for visually completed contours. *Current Biology*, 10(11):663–666.

Goodell, B. and Rainville, S. (2009). Critique of a wilson-cowan model linking neural synchronization with visual grouping. In *CVR Conference*, York University: Toronto, ON.

Gray, C. M. (1999). The temporal correlation hypothesis of visual feature integration: Still alive and well. *Neuron*, 24:31–47.

Gray, C. M., König, P., Engel, A. K., and Singer, W. (1989). Oscillatory responses in cat visual cortex exhibit inter-columnar synchronization which reflects global stimulus properties. *Nature*, 338:334–337.

Halgren, E., Mendola, J., Chong, C., and Dale, A. (2003). Cortical activation to

illusory shapes as measured with magnetoencephalography. *Neuroimage*, 18:1001–1009.

Heeger, D. J. (1987). Model for the extraction of image flow. *Journal of the Optical Society of America A*, 4(8):1455–1471.

Heeger, D. J. (1992). Normalization of cell responses in cat striate cortex. *Vis. Neurosci.*, 9:181–197.

Heider, B., Meskenaite, V., and Peterhans, E. (2000). Anatomy and physiology of a neural mechanism defining depth order and contrast polarity at illusory contours. *Eur. J. Neurosci.*, 12:4117–4130.

Herculano-Houzel, S., Munk, M. H. J., Neuenschwander, S., and Singer, W. (1999). Precisely synchronized oscillatory firing patterns require electroencephalographic activation. *The Journal of Neuroscience*, 19:3992–4010.

Hindmarsh, J. L. and Rose, R. M. (1982). A model of the nerve impulse using two first-order differential equations. *Nature*, 296:162–164.

Hindmarsh, J. L. and Rose, R. M. (1984). A model of neuronal bursting using three coupled first order differential equations. *Proceedings of the Royal Society of London: B*, 221:87–102.

Hirsch, J., DeLaPaz, R., Relkins, N., Victor, J., Kim, K., Li, T., Borden, P., Rubin, N., and Shapley, R. (1995). Illusory contours activate specific regions in human visual cortex: evidence from functional magnetic resonance imaging. *Proceedings of the National Academy of Sciences of the United States of America*, 92:6469–6473.

Hodgkin, A. L. and Huxley, A. F. (1952). A quantitative description of membrane current and its application to conduction and excitation in nerve. *J. Physiol*, 117:500–544.

Hogben, J. H. and Di Lollo, V. (1974). Perceptual integration and perceptual segregation of brief visual stimuli. *Vision Research*, 14:1059–1069.

Hramov, A. E. and Koronovskii, A. A. (2004). An approach to chaotic synchronization. *Chaos: An Interdisciplinary Journal of Nonlinear Science*, 14:603–613.

Hubel, D. H. and Wiesel, T. N. (1962). Receptive fields, binocular interaction and functional architecture in the cat's visual cortex. *Journal of Physiology*, 160:106–154.

Hubel, D. H. and Wiesel, T. N. (1968). Receptive fields and functional architecture of monkey striate cortex. *Journal of Physiology*, 195:215–243.

Hutcheon, B. and Yarom, Y. (2000). Resonance, oscillation and the intrinsic frequency preferences of neurons. *Trends in Neurosciences*, 23:216–222.

Izhikevich, E. M. (2004). Which model to use for cortical spiking neurons? *IEEE Transactions on Neural Networks*, 15(5):1063–1070.

Izhikevich, E. M. (2006). *Dynamical Systems in Neuroscience: The Geometry of Excitability and Bursting.* The MIT Press, Cambridge, MA.

Izhikevich, E. M., Desai, N. S., Walcott, E. C., and Hoppensteadt, F. C. (2003). Bursts as a unit of neural information: selective communication via resonance. *Trends in Neurosciences*, 26(3):161–167.

Jensen, O. and Lisman, J. E. (1998). An oscillatory short-term memory buffer model can account for data on the sternberg task. *Journal of Neuroscience*, 18:10688–10699.

Kandel, E. R., Schwartz, J. H., and Jessell, T. M. (2000). *Principles of Neural Science, Fourth Edition.* McGraw-Hill, New York.

Kandil, F. I. and Fahle, M. (2001). Purely temporal figure-ground segmentation. *European Journal of Neuroscience*, 13:2004–2008.

Kanizsa, G. (1976). Subjective contours. *Scientific American*, 234(4):48–52.

Kepler, T. B., Abbott, L. F., and Marder, E. (1992). Reduction of conductance-based neuron models. *Biological Cybernetics*, 66:381–387.

Koepsell, K., Wang, X., Hirsch, J., and Sommer, F. T. (2010). Exploring the function of neural oscillations in early sensory systems. *Frontiers in Neuroscience*, 4(1):53–61.

Koffka, K. (1935). *Principles of Gestalt Psychology.* Harcourt, Brace and World, New York.

Köhler, W. (1920). *Die physischen Gestalten in Ruhe und im stationären Zustand.* F. Vieweg, Braunschweig, Germany.

Kreiter, A. K. and Singer, W. (1996). Stimulus-dependent synchronization of neuronal responses in the visual cortex of the awake macaque monkey. *Journal of Neuroscience*, 16(7):2381–2396.

Kruger, N. (1998). Collinearity and parallelism are statistically significant second-order relations of complex cell responses. *Neural Processing Letters*, 8:117–129.

Kruggel, F., Herrmann, C., Wiggins, C., and von Cramon, D. (2001). Hemodynamic and electroencephalographic responses to illusory figures: recording of the evoked potentials during functional mri. *Neuroimage*, 14:13271336.

Lamme, V. A. F. and Spekreijse, H. (1998). Neuronal synchrony does not represent texture segregation. *Nature*, 396:362–366.

Larsson, J., Amunts, K., Gulyás, B., Malikovic, A., Zilles, K., and Roland, P. (1999). Neuronal correlates of real and illusory contour perception: functional anatomy with pet. *Eur. J. Neurosci.*, 11:4024–4036.

Lee, S. H. and Blake, R. (1999). Visual form created solely from temporal structure. *Science*, 284:1165–1168.

Lee, S. H. and Blake, R. (2001). Neural synergy in visual grouping: When good continuation meets common fate. *Vision Research*, 41:2057–2064.

Lennie, P. (2003). The cost of cortical computation. *Current Biology*, 13:493–497.

Lisman, J. E. (1996). Bursts as a unit of neural information: making unreliable synapses reliable. *Trends in Neurosciences*, 75:2467–2485.

Luck, S. J. and Vogel, E. K. (1997). The capacity of visual working memory for features and conjunctions. *Nature*, 390:279–281.

Mendola, J., Dale, A., Fischl, B., Liu, A., and Tootell, R. (1999). The representation of illusory and real contours in human cortical visual areas revealed by functional magnetic resonance imaging. *J. Neurosci.*, 19:8560–8572.

Morris, C. and Lecar, H. (1981). Voltage oscillations in the barnacle giant muscle fiber. *Biophysical Journal*, 35:193–213.

Munk, M. H. J., Roelfsema, P. R., König, P., Engel, A. K., and Singer, W. (1996). Role of reticular activation in the modulation of intracortical synchronization. *Science*, 272:271–274.

Murray, M. M., Foxe, D. M., Javitt, D. C., and Foxe, J. J. (2004). Setting boundaries: Brain dynamics of modal and amodal illusory shape completion in humans. *The Journal of Neuroscience*, 24(31):6898–6903.

Murray, M. M., Wylie, G. R., Higgins, B. A., Javitt, D. C., Charles E. Schroeder, 1, ., and Foxe, J. J. (2002). The Spatiotemporal Dynamics of Illusory Contour Processing: Combined High-Density Electrical Mapping, Source Analysis, and Functional Magnetic Resonance Imaging. *The Journal of Neuroscience*, 22(12):5055–5073.

Ohtani, Y., Okamura, S., Shibasaki, T., Arakawa, A., Yoshida, Y., Toyama, K., and Ejima, Y. (2002). Magnetic responses of human visual cortex to illusory contours. *Neurosci. Lett.*, 321:173176.

Olshausen, B. A. (2003). Learning sparse, overcomplete representaitons of time-varying natural images.

Parton, A., Donnelly, N., and Usher, M. (2001). The effects of temporal synchrony on the perceived organization of elements in spatially symmetric and asymmetric grids. *Visual Cognition*, 8:637–654.

Pegna, A., Khateb, A., Murray, M., Landis, T., and Michel, C. (2002). Neural processing of illusory and real contours revealed by high-density erp mapping. *NeuroReport*, 13:965–968.

Pelli, D. G. (1997). The videotoolbox software for visual psychophysics: Transforming numbers into movies. *Spatial Vision*, 10:437–442.

Peterhans, E. and Heitger, F. (2001). Simulation of neuronal responses defining depth order and contrast polarity at illusory contours in monkey area v2. *J. Comput. Neurosci.*, 10:195–211.

Prazdny, K. (1983). Illusory contours are not caused by simultaneous brightness contrast. *Percept. Psychophys.*, 34:403–404.

Prazdny, K. (1986). Illusory contours from inducers defined solely by spatiotemporal correlation. *Percept. Psychophys.*, 39:175–178.

Rager, G. and Singer, W. (1998). The response of cat visual cortex to flicker stimuli of variable frequency. *European Journal Of Neuroscience*, 10:1856–1877.

Rainville, S. and Clarke, A. (2008). Distinct perceptual grouping pathways revealed by temporal carriers and envelopes. *Journal of Vision*, 8(15):1–15.

Rall, W. (1967). Distinguishing theoretical synaptic potentials computed for different soma-dendritic distributions of synaptic input. *Journal of Neurophysiology*, 10:1138–1168.

Reichardt, W. (1969). Movement perception in insects. In Reichardt, W., editor, *Processing of Optical Data by Organisms and Machines*, pages 465–493. Academic Press, London, New York.

Rieke, F., Warland, D., de Ruytervan Steveninck, R. R., and Bialek, W. (1997). *Spikes: Exploring the Neural Code*. MIT Press, Boston, MA.

Rinzel, J. (1985). Excitation dynamics: insights from simplified membrane models. *Federation proceedings*, 44:2944–2946.

Rinzel, J. and Ermentrout, G. B. (1989). *Analysis of neural excitability and oscillations*. MIT Press, Cambridge, MA, USA.

Ritzl, A., Marshall, J., Weiss, P., Zafiris, O., Shah, N., Zilles, K., and Fink, G. (2003). Functional anatomy and differential time courses of neural processing for explicit, inferred, and illusory contours. an event related fmri study. *Neuroimage*, 19:1567–1577.

Robson, J. G. (1966). Spatial and temporal contrast-sensitivity functions of visual system. *Journal of the Optical Society of America*, 56(8):1141–1142.

Rodieck, R. W. (1991). Which cells code for color? In Valberg, A. and Lee, B. B., editors, *From Pigments to Perception: Advances in Understanding Visual Processes*, pages 83–93. Plenum Press, London.

Roelfsema, P. R., Engel, A. K., König, P., and Singer, W. (1997). Visuomotor integration is associated with zero timelag synchronization among cortical areas. *Nature*, 385:157–161.

Rogers-Ramachandran, D. C. and Ramachandran, V. S. (1998). Psychophysical evidence for boundary and surface systems in human vision. *Vision Research*, 38:71–77.

Rose, R. M. and Hindmarsh, J. L. (1989). The assembly of ionic currents in a thalamic neuron i. the three-dimensional model. *Proceedings of the Royal Society of London. Series B, Biological Sciences*, 237(1288):267–288.

Seghier, M., Dojat, M., Delon-Martin, C., Rubin, C., Warnking, J., Segebarth, C., and Bullier, J. (2000). Moving illusory contours activate primary visual cortex: an fmri study. *Cereb. Cortex*, 10:663–670.

Sekuler, A. B. and Bennett, P. J. (2001). Generalized common fate: Grouping by common luminance changes. *Psychological Science*, 12(6):437–444.

Shalden, M. N. and Movshon, J. A. (1999). Synchrony unbound: A critical evaluation of the temporal binding hypothesis. *Neuron*, 24:67–77.

Shapley, R. and Gordon, J. (1985). Nonlinearity in the perception of form. *Percept. Psychophys.*, 37:84–88.

Sherman, S. M. (1996). Dual response modes in lateral geniculate neurons: mechanisms and functions. *Visual Neuroscience*, 13:205–213.

Sherman, S. M. (2001). Tonic and burst firing: dual modes of thalamocortical relay. *Trends in Neuroscience*, 24:122–126.

Sigman, M., Cecchi, G. A., Gilbert, C. D., and Magnasco, M. O. (2001). On a common circle: Natural scenes and gestalt rules. *Proceedings of the National Academy of Sciences, U.S.A.*, 27(4):1935–1940.

Simoncelli, E. P. and Heeger, D. J. (1998). A model of neuronal responses in visual area mt. *Vision Research*, 38(5):743–761.

Singer, W. (1999). Neuronal synchrony: a versatile code for the definition of relations? *Neuron*, 24:49–65.

Singer, W. (2004). Synchrony, oscillations, and relational codes. In Chalupa, L. M. and Werner, J. S., editors, *The Visual Neurosciences*, chapter 113, pages 1665–1682. The MIT Press, Cambridge, Massachusetts.

Spehar, B. (2000). Degraded illusory contour formation with non-uniform inducers in kanizsa configurations: the role of contrast polarity. *Vision Research*, 40:2653–2659.

Stanley, D. and Rubin, N. (2003). fmri activation in response to illusory contours and salient regions in the human lateral occipital complex. *Neuron*, 37:323–331.

Steinmetz, P. N., Roy, A., Fitzgerald, P. J., Hsiao, S. S., Johnson, K. O., and Niebur, E. (2000). Attention modulates synchronized neuronal firing in primate somatosensory cortex. *Nature*, 404:187–190.

Sterling, P. (2004). How retinal circuits optimize the transfer of visual information. In Chalupa, L. M. and Werner, J. S., editors, *The Visual Neurosciences*, chapter 17, pages 234–259. The MIT Press, Cambridge, Massachusetts.

Stevens, C. F. and Zador, A. M. (1998). Input synchrony and the irregular firing of cortical neurons. *Nature Neurosicence*, 1(3):210–217.

Stork, D. G. and Wilson, H. R. (1990). Do gabor functions provide appropriate descriptions of visual cortical receptive fields? *Journal of the Optical Society of America A*, 7(8):1362–1373.

Usher, M. and Donnelly, N. (1998). Visual synchrony affects binding and segmentation in perception. *Nature*, 394:179–182.

Victor, J. and Conte, M. (1998). Quantitative study of effects of inducer asynchrony on illusory contour strength. *Invest. Ophthalmol. Vis. Sci.*, 39:S206.

von der Malsburg, C. (1981). *The correlation theory of brain function.* MPI Biophysical Chemistry, Internal Report. Reprinted in Models of Neural NEtworks II (1994), E. Domany, J. L. van Hemmen and K. Schulten editors. Springer, Berlin.

Ware, C. (1981). Subjective contours independent of subjective brightness. *Perceptual Psychophysics*, 29:500504.

Wertheimer, M. (1938). Laws of organization in perceptual forms. In Ellis, W., editor, *A source book of Gestalt psychology*, chapter 113, pages 71–88. Routledge and Kegan Paul, London.

Wilson, H. R. (1978). Quantitative prediction of line spread function measurements: implications for channel bandwidths. *Vision Research*, 18:493–496.

Wilson, H. R. (1999). *Spikes, Decisions, and Actions: The Dynamical Foundations of Neuroscience.* Oxford University Press, New York.

Wilson, H. R. and Gelb, D. J. (1984). Modified line-element theory for spatial-

frequency and width discrimination. *Journal of the Optical Society of America A*, 1:124–131.

Wilson, H. R., McFarlane, D. K., and Phillips, G. C. (1983). Spatial frequency tuning of orientation selective units estimated by oblique masking. *Vision Research*, 23(9):873–882.

Yen, S.-C., Menschik, E. D., and Finkel, L. H. (1999). Perceptual grouping in striate cortical networks mediated by synchronization an desynchronization. *Neurocomputing*, 26027:609–616.

Zhou, H., Friedman, H., and von der Heydt, R. (2000). Coding of border ownership in monkey visual cortex. *J. Neurosci.*, 20:6594–6611.